Phase transition and hysteresis in an ensemble of stochastic spiking neurons

Andreas Kaltenbrunner[1,2,*], Vicenç Gómez[1,2] and Vicente López[1,2]

[1]*Universitat Pompeu Fabra, Departament de Tecnologia, Passeig de Circumval·lació 8, 08003 Barcelona, Spain*

[2]*Barcelona Media Centre d'Innovació, Ocata 1, 08003 Barcelona, Spain*

June 11, 2007

Abstract

An ensemble of stochastic non-leaky integrate-and-fire neurons with global, delayed and excitatory coupling and a small refractory period is analyzed. Simulations with adiabatic changes of the coupling strength indicate the presence of a phase transition accompanied by a hysteresis around a critical coupling strength. Below the critical coupling production of spikes in the ensemble is governed by the stochastic dynamics whereas for coupling greater than the critical value the stochastic dynamics looses its influence and the units organize into several clusters with self-sustained activity. All units within one cluster spike in unison and the clusters themselves are phase-locked. Theoretical analysis leads to upper and lower bounds for the average inter-spike interval of the ensemble valid for all possible coupling strengths. The bounds allow to calculate the limit behavior for large ensembles and characterize the phase transition analytically. These results may be extensible to pulse coupled oscillators.

Keywords: phase transition; hysteresis; stochastic neurons; pulse coupled oscillators; self-organization; synchronization

1   Introduction

The collective dynamics of networks composed of neuron-like elements which interchange messages have been studied in many areas of science. Several models have been developed to simulate and analyze phenomena produced by pacemaker cells in heart (Peskin, 1975), neurons in the brain (Bienenstock, 1995), swarms of fireflies (Buck, 1988; Copeland & Moiseff, 1995) or hand clapping of opera theater attendants (Néda et al., 2000). Synchronization of the ensemble units is a common characteristic of these phenomena.

The observed synchronization effects are different according to the model characteristics. Most studies consider only instantaneous coupling (i.e no delay in the message exchange) between the units which simplifies the analysis of the resulting dynamics. Under this restriction Mirollo and Strogatz (1990) demonstrated that certain types of identical leaky oscillators with global coupling synchronize for almost all initial conditions. Their result has been extended by Senn and Urbanczik (2000) allowing non-identical oscillators whose intrinsic frequencies, thresholds and couplings are heterogeneous within a certain range. They showed that non-leaky linear integrate-and-fire neurons synchronize for any initial condition for almost all parameter values of the system and speculate that, using perturbative arguments, their results might be still valid in the presence of a small leakiness. The influence of an absolute refractory period on the Mirollo-Strogatz model

---

*Corresponding author: e-mail: andreas.kaltenbrunner@upf.edu; Fax: +34 93 542 2517

has been analyzed by Chen (1994) and Kirk and Stone (1997). The authors of these papers showed that the system approaches synchrony for almost all initial conditions if the refractory period is below a critical value.

If a delay for the message exchange is added more complex forms of synchronization are observed. Ernst et al. (1998) showed empirically that for both, excitatory and inhibitory coupling, the neurons tend to cluster their activities. All neurons within a cluster are synchronized and fire in unison whereas the clusters are phase-locked with constant phase differences. The number of clusters of the system was inversely proportional to the length of the delay for inhibitory coupling. The stability of these clusters was analyzed in (Timme et al., 2002) and similar phenomena were observed by van Vreeswijk (1996) for coupling with α functions and have been proposed as a possible mechanism for neural information coding and processing in the form of synfire chains (Abeles, 1991; Bienenstock, 1995; Diesmann et al., 1999) and (Ikegaya et al., 2004). The importance of delay for neural modeling has recently been addressed by Izhikevich et al. (2004) and Izhikevich (2006), claiming that it allows an unprecedented information capacity, which translates into an increase of stable firing patterns in more realistic neural populations due to heterogeneous delays.

In this study we investigate the influence of variations in the coupling strength on a network of non-leaky integrate-and-fire neurons with delayed, pulsed coupling and a small refractory period. We show that a system of these characteristics exhibits a phase transition with a delay-induced hysteresis. Phase transition phenomena are well known in populations of weakly coupled oscillators, where the onset of synchronization represents a second order phase transition analogous to the formation of a Bose-Einstein condensate (Winfree, 1967; Kuramoto, 1984). Interacting chaotic oscillators also exhibit a special kind of phase transition which closely resembles that seen in spin glasses (Kaneko, 1990). Recent work analyzes the existence of phase transitions for chains (Östborn, 2002) and lattices (Östborn et al., 2003) of pulse-coupled oscillators with a particular, biologically inspired phase response curve.

Contrary to the former mentioned studies the neurons of the network we analyze are driven by stochastic input, i.e. pulse-coupled oscillators with stochastic frequencies. Such type of model neurons have been introduced in (Gerstein & Mandelbrot, 1964) and one possible interpretation of the stochasticity is random input form background neurons that are not explicitly modeled (Stein, 1967). The units perform a random walk towards a threshold and, according to the characteristics of the stochastic input, several studies have analyzed the resulting distributions of the inter-spike intervals of single units for the case of non-leaky integrate-and-fire (IF) neurons[1] (Tuckwell et al., 1988; Fusi & Mattia, 1999; Salinas & Sejnowski, 2002; Middleton et al., 2003; Lindner, 2004). For a review on those results and the more biological plausible models of leaky IF neurons see (Burkitt, 2006) and the references therein.

Here we are interested in a network of such units which can be interpreted as a simplified model of a pool of globally coupled neurons with similar properties, which receive stochastic input form different regions of the brain (Gerstner, 2000). Such networks have been studied for the cases of inhibitory (Brunel & Hakim, 1999; Brunel & Hansel, 2006) and excitatory coupled (Gerstner, 2000) leaky IF neurons. The later work mainly concentrated on noise in the thresholds or the refractoriness and only makes some comments on the effect of stochastic inputs. A combination of excitatory and inhibitory coupling, where noise leaded to enhanced stability of long distance synchronization, has been analyzed in a realistic heterogeneous neural model (Hodgkin-Huxley) by (McMillen & Kopell, 2003).

A common problem of these more biologically plausible models is that analytical stud-

---

[1]Sometimes also referred to as leak-less or perfect integrator neurons.

ies are hard to perform especially if delay and refractory period are added. To bypass this problem we base our analysis on a discrete-time model introduced in Rodríguez et al. (2001), of globally coupled, non-leaky integrate-and-fire neurons with a constant transmission delay and a refractory period, where the stochastic inputs to the units are provided by a Bernoulli process. This model allows efficient simulations and a detailed analytical study and is an extension of the discrete model presented in (van Vreeswijk & Abbott, 1993).

The use of a stochastic model allows to observe that the nature of the dynamics changes abruptly from a regime where the units show noisy, irregular spiking behavior at low coupling to a regime with deterministic, self-sustained and repetitive spiking behavior if the coupling is increased to values greater than the critical coupling strength. There the units organize into several clusters, have all the same inter-spike interval (ISI), fire in-phase with the units of their own cluster and phase-locked with constant time differences to the neurons of other clusters. The clusters are robust to modifications of the rate of the stochastic input. If the coupling strength is increased even more, the number of clusters and the length of the ISI decrease since some clusters merge, but the system continues with the phase-locked firing. If, on the contrary, the coupling is decreased, the units of the population remain firing phase-locked without an increase of the ISI or the number of clusters until the critical coupling strength is reached, where the clusters start to dissolve. Thus a hysteresis effect can be observed.

The phase transition and the hysteresis can be described in detail. Upper and lower bounds for the ISI as well as an approximation for the mean ISI are obtained and the system's behavior for large ensemble sizes (i.e. at its thermodynamic limit) is characterized.

We conjecture that the observed phenomena can potentially occur in rather different models with a refractory period and delayed coupling. The results may be useful to explain certain aspect of animal behavior e.g. synchronized and non-synchronized flashing of North American fireflies (Copeland & Moiseff, 1995), create a simple working-memory (Wang, 2001) and may be applied in information processing.

The rest of this work is organized as follows: We first give an overview over the model in section 2 and explain the methodology we used for the experiments in section 3. In section 4 we present experimental and analytical results for homogeneous networks which are extended to heterogeneous networks in section 5. Section 6 shows the results can be obtained using either parallel or sequential updating. Finally, the findings are discussed in section 7 and some derivations of formulas will be presented in the appendix.

2   Description of the model

The discrete neural model studied in this work is based on the one introduced by Rodríguez et al. (2001) which is an extension of the work of van Vreeswijk and Abbott (1993). It is composed of a globally coupled network of N non-leaky stochastic integrate-and-fire units. Unlike the model of Rodríguez et al. (2001), where only a finite number of states is allowed, each unit i is at time t in a continuous state $a_i(t) \in [1, \infty)$. Transitions between states can take place only at discrete time-steps and are limited by a threshold L. L is a positive real number and limits the range of excitations in the sense that every state $a_i(t) \geq L$ is meta-stable since it absorbs any further state transitions or incoming messages and relaxes to 1 after the end of a refractory period t_{ref}.

We have two types of state transitions:

1. Stochastic state transitions:
   At every discrete time-step t a single unit can increase its state variable by 1 with

probability p if the state of the neuron is below threshold L.

$$a_i(t+1) = \begin{cases} a_i(t) + 1 & \text{with probability } p \\ a_i(t) & \text{with probability } (1-p) \end{cases} \quad \text{if } a_i(t) < L,$$
$$a_i(t + t_{ref}) = 1 \text{ with probability } 1 \qquad\qquad\qquad\qquad \text{if } a_i(t) \geq L. \tag{2.1}$$

2. State transitions due to coupling between units:
   A unit j that reaches the threshold L at time t emits a spike and increases the continuous state variable of an unit i by an amount ϵ_{ij} at time $t + \delta$, where δ stands for the synaptic delay. Rodríguez et al. (2001) only allowed positive integer values for ϵ_{ij}. We will not use this restriction and allow any non-negative real number. The total amount of change of a single unit at time $t + \delta$ is obtained by summing over all neurons which had reached the threshold at time t. This gives us the following transition function due to messages of other units (we have to consider three cases depending on the threshold situation and the relation of t_{ref} and δ):

$$a_i(t+\delta) = \begin{cases} a_i(t) + \sum_{j=1}^{N} \epsilon_{ij} \Theta_L(a_j(t)) & \text{if } a_i(t) < L, \\[2mm] 1 + \sum_{j=1}^{N} \epsilon_{ij} \Theta_L(a_j(t)) & \text{if } a_i(t) \geq L \text{ and } \delta \geq t_{ref}, \\[2mm] 1 & \text{if } a_i(t) \geq L \text{ and } \delta < t_{ref}. \end{cases} \tag{2.2}$$

Notice that $\Theta_L(x) = \Theta(x - L)$ where $\Theta(x)$ is the Heaviside step function whose value is 0 for negative inputs and 1 elsewhere. We use this function to sum only over the neurons which reached threshold L in the previous time-step.

We restrict our analysis to the case of $\delta \geq t_{ref}$. Consequences of other choices are discussed at the end of the paper. To keep the simulations simple we set both t_{ref} and δ equal to 1, which allows us to combine these two types of evolution (2.1) and (2.2) into a single equation and we get the following dynamics:

$$a_i(t+1) = \begin{cases} a_i(t) + \sum_{j=1}^{N} \epsilon_{ij} \Theta_L(a_j(t)) + 1 & \text{with probability } p \\ a_i(t) + \sum_{j=1}^{N} \epsilon_{ij} \Theta_L(a_j(t)) & \text{with probability } (1-p) \end{cases} \quad \text{if } a_i(t) < L,$$
$$a_i(t+1) = 1 + \sum_{j=1}^{N} \epsilon_{ij} \Theta_L(a_j(t)) \text{ with probability } 1 \qquad\qquad \text{if } a_i(t) \geq L. \tag{2.3}$$

Rodríguez et al. (2001) set all $\epsilon_{ij} = \epsilon$ for $i \neq j$ and all $\epsilon_{ii} = 0$. With these prerequisites the parameter

$$\eta = \frac{L-1}{(N-1)\epsilon} \tag{2.4}$$

was introduced to characterize the strength of the interactions among the units. The parameter η gives the ratio between the total change in activation needed for a neuron to fire and the one provided by the the coupling with the rest of the population. For $\eta \gg 1$ the following expressions approximate well the mean and standard deviation of the ISI of a neuron in the ensemble:

$$\tau_{mf} = t_{ref} + \frac{L - (N-1)\epsilon - 1}{p} \; , \qquad \sigma_{mf} = \frac{\eta - 1}{\eta} \frac{\sqrt{(L - (N-1)\epsilon - 1)(1-p)}}{p} \; . \tag{2.5}$$

4

Details and derivations of these equations, which are based on a mean-field approach, replacing the state transitions due to coupling between units by their average, can be found in (Rodríguez et al., 2001)[2]. Equations (2.5) fail to describe the behavior of the system in regions of high coupling. At $\eta = 1$ they predict one giant cluster containing all the units with an ISI of 1. This would only be true for a system without delay and refractory period. In our system, however, the more important correlations due to the delayed message exchange become (i.e. the smaller becomes η), the bigger is the difference between τ_{mf} and the ISI of the units. This was first reported by Rodríguez et al. (2002), who found that for $\eta = 1$ after an initial transient the system reaches one of a large number of periodic firing patterns, composed of several clusters. The same is true for $\eta < 1$, as can be observed in Figure 1, where raster plots of spikes of a system consisting of 100 neurons are shown. The irregular behavior of the system at $\eta = 1.2$ (Figure 1a) changes into a regular repetitive spiking pattern at $\eta = 1$ (Figure 1b) if the coupling is increased. If increased further some clusters merge but the system continues with the phase-locked clustered firing as shown in Figure 1c for $\eta = 0.9$.

---

[2]Note that (Rodríguez et al., 2001) used $t_{ref} = 1$ in their analysis, which can be easily extended to the general case of t_{ref} variable.
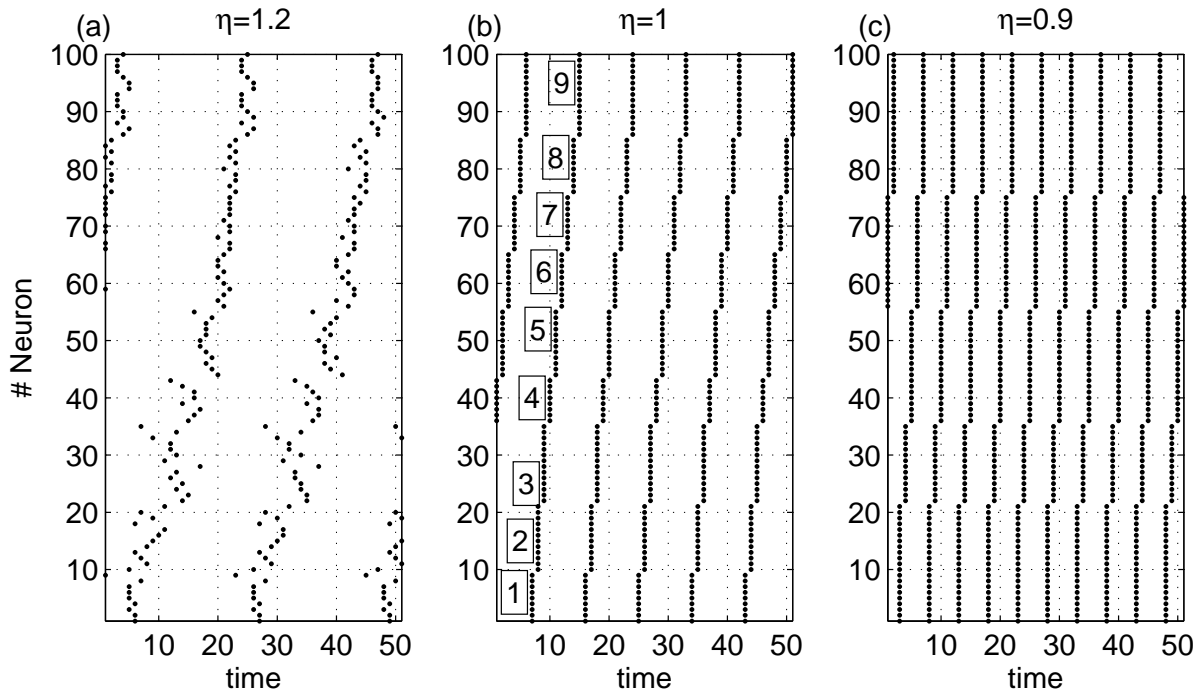

Figure 1: Raster plot of spikes (firing patterns) of 100 neurons (noise rate $p = 0.9$ and threshold $L = 100$) for different values of η. Simulation started with a random initial state for every neuron. Coupling strength is slowly increased every 100 time-steps and time was set to 0 after a transient of 50 time-steps. For clarity in the visualization the neurons are re-labeled according to their spike-time at $\eta = 1$. **(a)** We observe irregular firing at $\eta = 1.2$. **(b)** At $\eta = 1$ the neurons organize into 9 phase-locked clusters (labeled by the boxed numbers). **(c)** At $\eta = 0.9$ the number of phase-locked clusters is reduced to 5 since clusters number 1, 2; 4, 5; 6, 7 and 8, 9 merged into new bigger clusters. Note that the length of the ISI coincides with the number of clusters for $\eta = 1$ and $\eta = 0.9$.

5

3   Experimental Setup

To analyze the system described in section 2 we use the following experimental procedures. The phase transition and the hysteresis are best understood observing how the system reacts to adiabatic[3] changes of the coupling strength. A simple analogy is useful to understand the procedure. Consider a cloud of particles that is slowly concentrated or diluted by increasing or decreasing the volume. We begin with a very dispersed cloud with little interaction between the particles and start to concentrate it in a stepwise manner. At every concentration step the interaction among the particles increases. At some point the process is inversed and the cloud is diluted again until reaching the original state. We therefore distinguish two different processes in our experiments, to which we refer as *concentration process* and *dilution process*. The particles are in our case the spiking units and the interaction can be measured via the relation of the threshold L and the coupling strength ϵ multiplied by the number of units N. As explained above (see equation (2.4)) this relation is reflected in the parameter η, which in our analogy represents the volume of the system.

In our experiments we choose a fixed set of N neurons with fixed threshold L. The only parameter allowed to change is the global interaction strength ϵ. We start with units at random initial states and at regions of high η (usually $\eta = 2$) where the system can be described with high accuracy by equations (2.5) and is ergodic in the sense that all accessible micro-states are visited over a long period of time. The units in these regions can be viewed as nearly independent with a threshold lowered by the mean activity induced by messages received from other units. The only difference to real independence is a period focusing effect described by Rodríguez et al. (2001). This results in a slightly lower (by a factor $(\eta - 1)/\eta$ standard deviation than the one of an independent unit with lowered threshold.

Once an experiment is started we let the system evolve enough time-steps to avoid dependence on unnatural initial conditions (i.e. conditions that are not typical of the system) and let the ISI stabilize. Now we can start the concentration process by decreasing η in a stepwise manner. We achieve this via adapting ϵ. Notice that, although we change η by a constant $\Delta\eta$, the changes of ϵ are not constant due to the inverse relation of η and ϵ. After every decrease of η we let the system evolve enough time-steps until the ISI stabilizes again. This procedure is repeated until a value of η in the range between 1 and 0.5 is reached. Then we reverse the procedure and start the dilution process. We increase η in a stepwise manner until we reach again the starting value of η.

To analyze the results we calculate two types of statistics of the ISIs of the units for every value of η.

1. The statistics of the ISI of the units just before the parameters of the system are changed (i.e. ϵ is increased or decreased). We call the first two moments of these statistics τ and σ (τ denotes the mean ISI of the ensemble and σ their standard deviation).

2. The statistics of τ and σ of different experiments: We call $\langle\tau\rangle$ the mean and σ_{exp} the standard deviation of the ensemble's mean ISI τ. In the case of σ we only calculate its mean value, which we denote $\langle\sigma\rangle$.

The value of $\langle\sigma\rangle$ gives us an idea of the likelihood to end up firing with phase-locked clusters for the given parameter values. The closer $\langle\sigma\rangle$ is to 0 the bigger is this likelihood.

---

[3]We use the term *adiabatic* as it is used in quantum mechanics, meaning a "sufficiently slow" change of the system.

If the units in one experiment have all the same ISI their standard deviation σ equals 0. σ_{mf} of equation (2.5) estimates $\langle\sigma\rangle$.

On the other hand, σ_{exp} measures the influence of the initial conditions and variations in the stochastic state transitions on the mean ISI τ of the ensemble.

4   Results

In this section we first present the outcome of several experiments that reveal the existence of a phase transition phenomenon of the system described in section 2 around a critical value of the coupling parameter η. This phenomenon is accompanied by a hysteresis effect which will also be described. We then give analytical bounds for the mean ISI $\langle\tau\rangle$. This description allows us to calculate the behavior of the observed phenomena for $N \to \infty$. We will refer to this limit behavior as thermodynamic limit in the rest of this work.
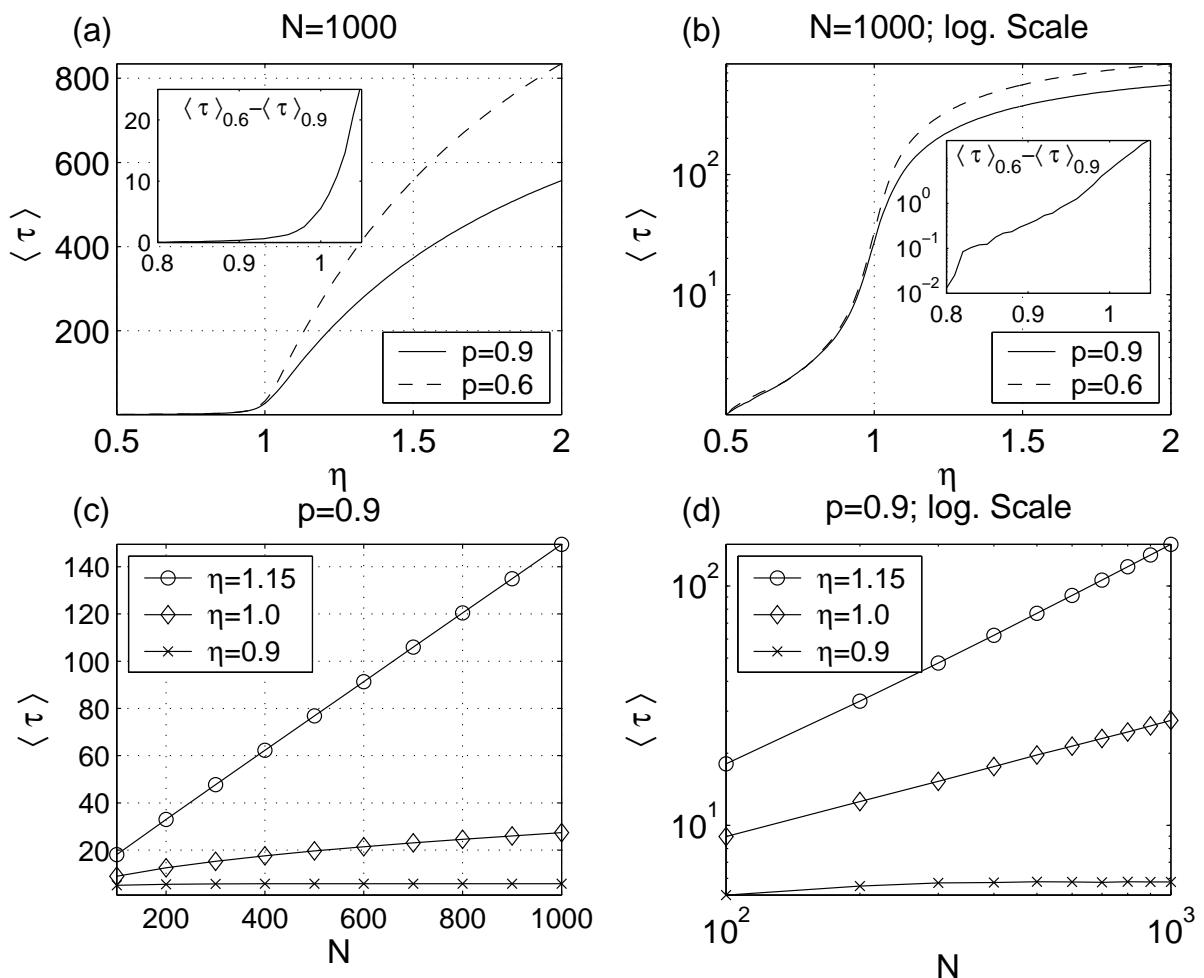

Figure 2: Mean ISI: Values of the ISI $\langle\tau\rangle$ over all neurons and 1000 experiments for increasing ϵ (i.e. decreasing η). Number of neurons $N = 1000$ equals threshold L in all cases. **(a)** Dependence of $\langle\tau\rangle$ on η for two different noise levels p. Inset shows the difference of both curves in the interesting region around $\eta = 1$. **(b)** Same as (a) but in logarithmic scale. **(c)** Dependence of $\langle\tau\rangle$ on N for different values of η and $p = 0.9$. **(d)** Same as (c) but in logarithmic scale. We can see a linear dependence of $\langle\tau\rangle$ on N for $\eta = 1.15$, a square root dependence for $\eta = 1$ and nearly no dependence for $\eta = 0.9$.

4.1 Experimental Results

4.1.1 Dependence of the ISI on the coupling strength ϵ

As explained in the model section one of the quantities we are interested in this work is the ISI. Especially we want to know how it is modified by small changes of the coupling parameter η. We therefore performed several experiments for different ensemble sizes as described in section 3 and observed the dependence of the mean value of the ISI $\langle \tau \rangle$ on the coupling parameter η for different values of the rate p of the stochastic evolution. First we analyze only the concentration process, where we slowly increase the amount of coupling between the neurons. Since the coupling parameter η is inverse proportional to the coupling strength an increase of the coupling strength indicates a decrease of η.

Figure 2a and 2b show the results for 1000 such concentration experiments for noise rates of $p = 0.9$ (solid line) and $p = 0.6$ (dashed line). We used an ensemble size of $N = 1000$ neurons and can observe how the mean ISI $\langle \tau \rangle$ decreases as we increase the coupling. Initially at high values for η there is a clear dependence on the noise rate p
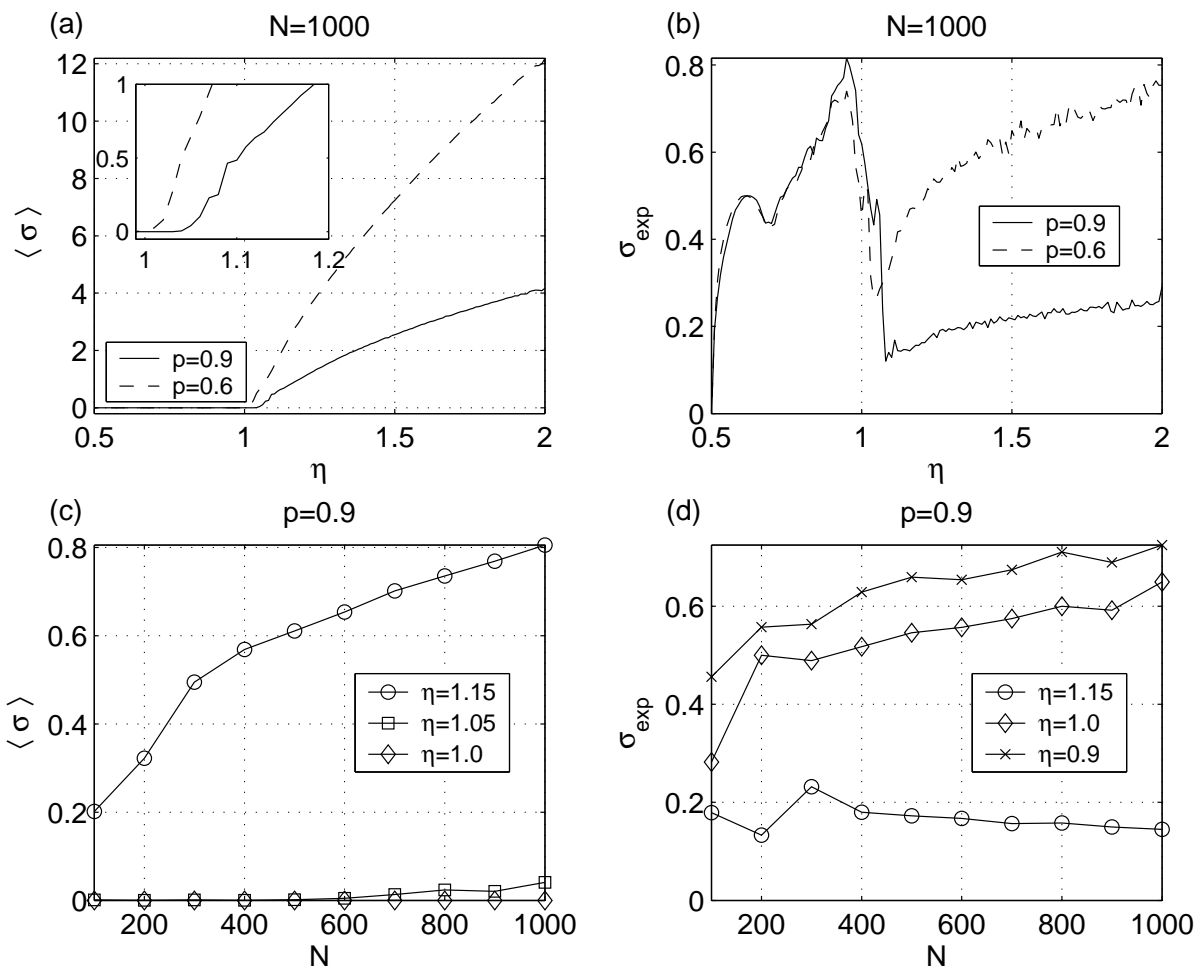

Figure 3: Standard Deviations: Values of the deviations of $\langle \sigma \rangle$ and σ_{exp} of the experiments with increasing ϵ (e.g. decreasing η) presented in Figure 2. Number of neurons N equals threshold L in all cases. **(a)** Dependence of $\langle \sigma \rangle$ on η for two different values of p. Inset shows a zoom on the interesting region around $\eta = 1$. **(b)** Same as (a) but for σ_{exp} **(c)** Dependence of $\langle \sigma \rangle$ on N for different values of η and $p = 0.9$. $\langle \sigma \rangle = 0$ for all $\eta < 1$ due to synchronization. **(d)** Dependence of σ_{exp} on N for different values of η and $p = 0.9$.

which seems to disappear as we reach $\eta = 1$. A closer examination of the mean ISIs of both experiments in this region reveals that their difference for η close to 1 and below decays exponentially to 0 with decreasing η. (Shown in the insets of Figures 2a and 2b). We will see later in the theoretical analysis that the greater N the faster is this decay and at the thermodynamic limit the mean ISI is independent of p for all values of $\eta < 1$.

When we analyze the deviation of the ISIs we also notice a change in the behavior of the system if we approach $\eta = 1$. The mean deviation $\langle \sigma \rangle$ of several experiments drops to 0 when the critical value of η is reached, indicating that the units organize into clusters and fire phase-locked, all with the same ISI. Figure 3a shows this effect for the concentration experiments with the two different noise rates analyzed before. In the inset we notice that for a noise level of $p = 0.9$ (solid line) the onset of phase-locking already happens at $\eta \approx 1.04$. This can also be observed in the deviation σ_{exp} of the experiments ISIs. Figure 3b shows the corresponding value of σ_{exp}. Here the onset of phase-locking is marked by an increase of σ_{exp}.

If the units are not phase-locked, σ_{exp} is low since it is the deviation of averages. Although there may be great differences between the ISIs of the units as is reflected by the value of $\langle \sigma \rangle$, once the mean ISI τ of the ensemble is calculated, these fluctuations are just averaged out. But as the units start to organize into phase-locked clusters the ensemble dynamics starts to govern the system. The deviation of the ensemble, σ, equals 0 but the deviation of the experiments, σ_{exp}, increases. The mean ISI τ of the ensemble is now an integer value, which depends on the evolution of all the units since the beginning of the experiment. This gives rise to a broader shape of the ISI distribution. Small fluctuations in the evolution of some units can lead to a different ISI of the whole system. Therefore the averaging effect observed before is lost and different experiments, although started with the same initial conditions, can lead to systems with different τ.

The maximum of σ_{exp} is reached when the rate p of the stochastic evolution looses most of its influence on the size of the ISI (Compare with Figure 2). In this sense the interval between the local minimum at $\eta > 1$ and maximum at $\eta < 1$ of σ_{exp} marks the transition between an ensemble governed by the stochastic evolution to an ensemble with self-sustained activity where the stochastic evolution does not have much influence on the statistics of the system. We can see that once the local maximum is reached the curves for $p = 0.9$ and $p = 0.6$ are practically identical if the system is further concentrated. (i.e the coupling strength is increased). σ_{exp} reaches a value of 0 at $\eta = 0.5$ when the system consists only of one giant cluster which spikes at every time-step. The strange bump at $\eta \approx 0.7$ can be explained by a probability of nearly 80% of having an ISI of 2 for this value of η. The value of σ_{exp} experiences thus an important decrease, but starts to increase again when the concentration continues and the probability of having an ISI of 1 increases.

4.1.2 Dependence of the ISI on the ensemble size N

Once the properties of the deviations have been described, our analysis focuses again on the mean ISI $\langle \tau \rangle$. The strange shape of the curves in the logarithmic scale of Figure 2b suggests that apart from the elimination of the dependency on the noise rate p something else is going on around the value of $\eta = 1$. To investigate this point further we observed the dependence of the ISI $\langle \tau \rangle$ on the ensemble size N.

Figures 2c and 2d reveal a quite different kind of dependence for different values of the coupling parameter η. For $\eta = 1.15$ (line with circles) we observe a linear dependence of $\langle \tau \rangle$ on N, whereas for $\eta = 0.9$ (line with crosses) the value of the ISI stabilizes once a certain number of neurons is in the ensemble ($N \geq 300$) and does not show any dependence

on the ensemble size. At $\eta = 1$ (line with diamonds) another type of relationship is observed. The slope in the double logarithmic scale of Figure 2d has nearly exactly a value of 0.5 indicating a relationship of type $\sqrt{N} \sim \langle \tau \rangle$.

The corresponding values of the deviations $\langle \sigma \rangle$ and σ_{exp} for $p = 0.9$ can be seen in Figures 3c and 3d. As expected for $\eta \leq 1$ the mean deviation $\langle \sigma \rangle = 0$ since the units fire phase-locked. We omit for clarity the line for $\eta = 0.9$ and only show the values for $\eta = 1$ (line with diamonds). For $\eta = 1.15$ (line with circles) we get a linear dependence of $\langle \sigma \rangle$ on $\sqrt{N}$ as predicted by Eq. (2.5). The additional curve for $\eta = 1.05$ (line with squares) allows to observe that the smaller the ensemble the earlier happens the onset of phase-locking in the concentration process. Here the units are phase-locked already for ensemble sizes of $N > 500$.

The dependence of σ_{exp} on N can be observed in Figure 3d. For $\eta = 1.15$ (line with circles), where the stochastic state transitions govern the ensemble, σ_{exp} slightly decreases since an increase of N implies an increase of the number of samples taken for every ISI τ and due to the central limit theorem a decrease of the deviation. For $\eta = 0.9$ (solid line with crosses) and $\eta = 1.0$ (solid line with circles) the σ_{exp} increases as N increases. This behavior changes in the case of $\eta = 0.9$, where σ_{exp} stabilizes for higher values of N and becomes independent of the ensemble size (data not shown).

4.2   Characterization of the Phase Transition

The results of the dependence of the mean ISI $\langle \tau \rangle$ on the ensemble size N for different values of η presented in Figures 2c and 2d motivate us to investigate if there exists a relation of type

$$\alpha N^c = \langle \tau \rangle \tag{4.1}$$

and analyze the dependence of c and α on the coupling parameter η. Equation (4.1) can be transformed into a linear equation with slope c and y-intercept α

$$\ln(\alpha) + c \ln(N) = \ln(\langle \tau \rangle). \tag{4.2}$$

This allows us to calculate c and α by least squares fits of the simulation data.

The results of these fits are shown in Figures 4 and 5. In both we see two curves, each represents a set of 10 different values of N. For every value of N the mean ISI $\langle \tau \rangle$ of 1000 concentration processes was calculated. For the solid line N takes values from 100 to 1000 in steps of 100 and for the dashed line values from 10^3 to 10^4. We can see that both c and α experience a sharp change of their value around $\eta = 1$. The higher the value of N the sharper this change is. We can therefore speak of a phase transition around a critical value of $\eta = 1$. We expect that for $N \to \infty$ the value of c should jump from 1 for $\eta > 1$ via 0.5 at $\eta = 1$ to 0 for $\eta < 1$.

The gray areas represent bounds obtained from theoretical analysis and will be discussed in section 4.3.

4.2.1   Hysteresis effect

After having analyzed the concentration process experimentally and characterized a phase transition phenomenon we are interested in what happens if we invert the process. Instead of increasing the coupling strength we decrease it in a stepwise manner. As described in section 3 we call this type of experiment dilution process. If we combine concentration and dilution process to obtain a cyclic process we notice a hysteresis effect comparing the mean ISIs $\langle \tau \rangle$ of both processes for values of η close to 1 and below.
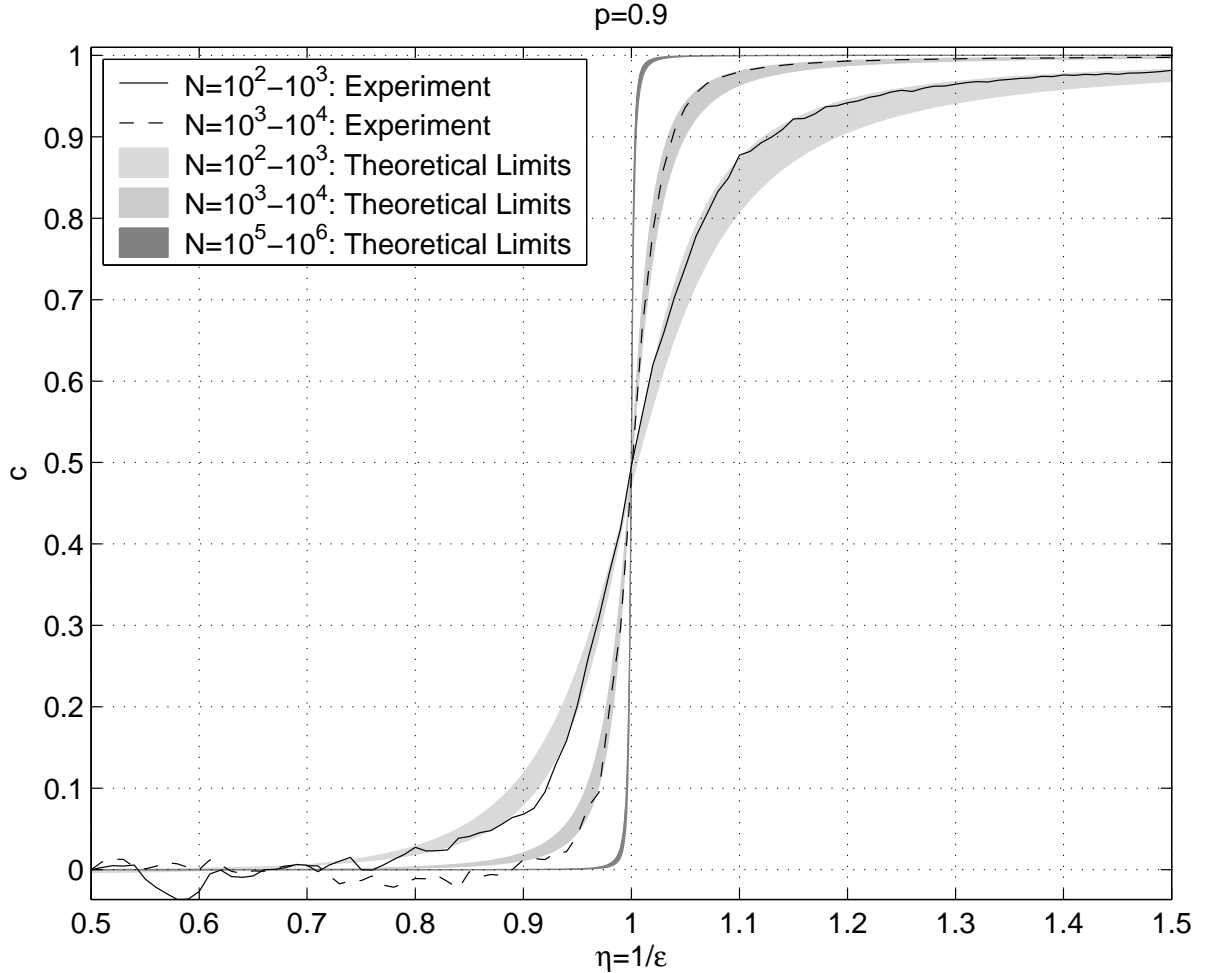
Figure 4: Comparison between experimental and theoretical results for the parameter c of the assumption that $\langle \tau \rangle = \alpha N^c$. 10 sets of 1000 experiments with $p = 0.9$ and different values for N were carried out. (Solid line: $N \in \{100, 200, \ldots 1000\}$. Dashed line: $N \in \{1000, 2000, \ldots 10000\}$). The values of c have been obtained by a least squares fit of the experiments with the linear equation $\ln(\langle \tau \rangle) = \ln(\alpha) + c \ln(N)$. The shaded areas show the region of possible values of c obtained by least squares fits of the theoretical bounds for $\langle \tau \rangle$ of equations (4.10) and (4.11)) and the assumption. For $N \in \{10^5, \ldots 10^6\}$ (darkest area), the value of c is already very close to its thermodynamic limit. The difference between the values of c of the two bounds is very low.

Figure 6 shows this effect for 3 different starting points of the dilution process. The dotted line represents the mean ISI $\langle \tau \rangle$ of the concentration process of 1000 experiments. When the concentration process stops and the dilution process is started, τ and therefore also $\langle \tau \rangle$ remain constant until a dilution of $\eta > 1$ is reached. The solid line with circles represents a dilution process stating at $\eta = 0.5$ and the dashed line with + markers one starting at $\eta = 0.9$. In both cases the ISI remains unchanged until $\eta = 1$ where it jumps then to a value slightly higher than the one predicted by the formulas (2.5) for this case. If we start the dilution process already at $\eta = 0.99$ we observe that $\langle \tau \rangle$ remains constant even for $\eta = 1.01$. Only if we dilute further $\langle \tau \rangle$ increases and starts to coincide with $\langle \tau \rangle$ of the other two dilution processes. Approximately at $\eta = 1.08$ the ISI of the dilution process coincides with the one of the concentration process. To understand this phenomenon in detail we carry out a theoretical analysis which will be presented in the next section.

4.3 Theoretical Description

Once identified the phenomena occurring in the model in experiments we make some theoretical observations to gain further insight. We base these observations on a deterministic approximation of the model where the stochastic evolution (2.1) of a neuron i is simplified into the following deterministic iterative rule:

$$
\begin{aligned}
a_i(t+1) &= a_i(t) + p & \text{if } a_i(t) < L, \\
a_i(t + t_{ref}) &= 1 & \text{if } a_i(t) \geq L.
\end{aligned}
\tag{4.3}
$$

The random walk performed by the units is replaced by their average behavior: a deterministic motion with constant homogeneous velocity p. An equivalent continuous time system but with heterogeneous velocities (frequencies) and without delay and refractory period has been studied by Senn and Urbanczik (2000). In the following we will restrict our analysis to the case where the delay δ of the message exchange is greater than or equal to the refractory period t_{ref}.
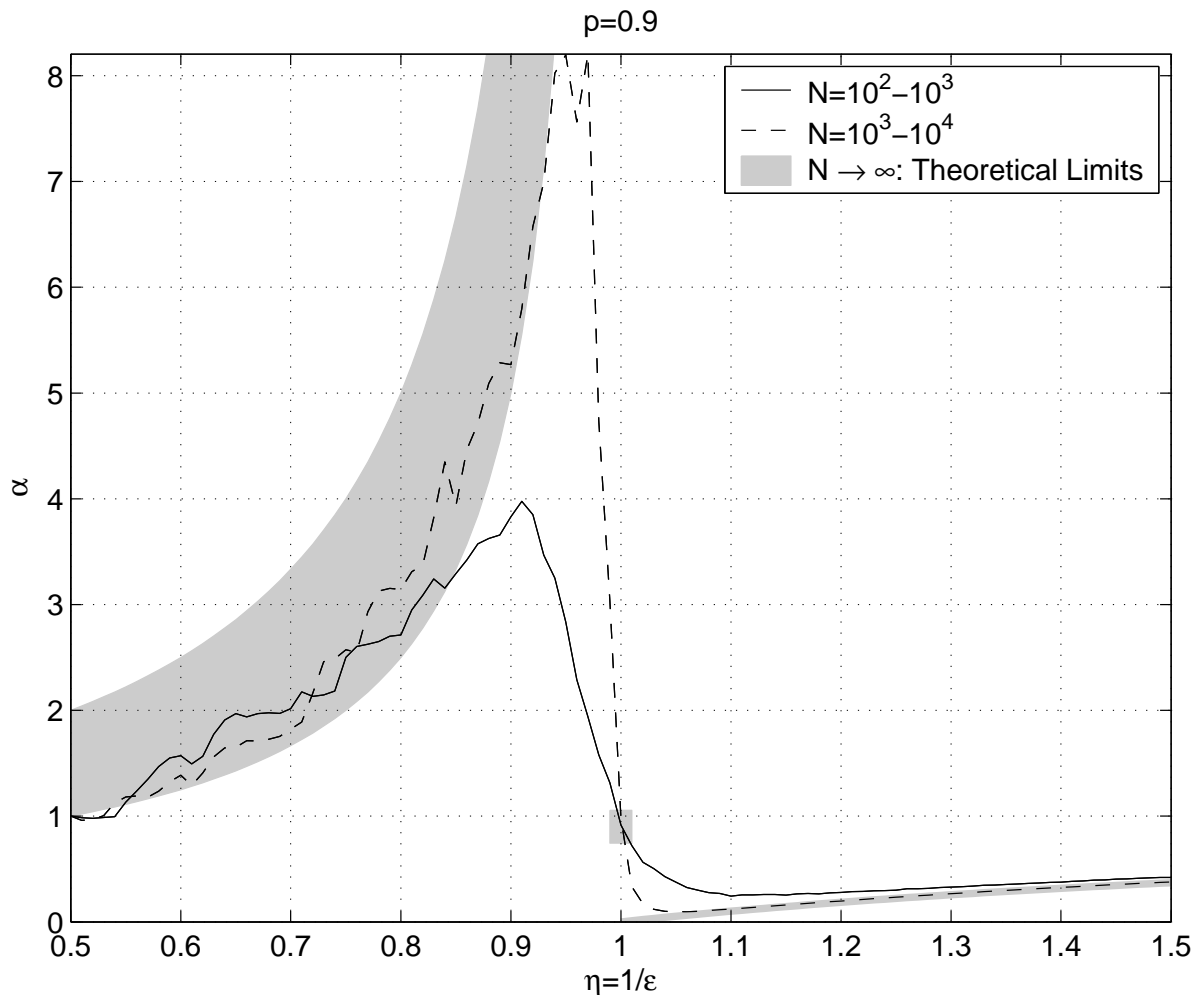

Figure 5: Comparison between experimental and theoretical results for the value α under the assumption that $\langle \tau \rangle = \alpha N^c$. 10 sets of 1000 experiments with $p = 0.9$ and different values for N were carried out. (Solid line: $N \in \{100, 200, \ldots 1000\}$. Dashed line: $N \in \{1000, 2000, \ldots 10000\}$). The values of α have been obtained by a least squares fit of the experiments with the equation $\ln(\langle \tau \rangle) = \ln(\alpha) + c \ln(N)$. The shaded areas show the regions of possible values of α for $N \to \infty$ according to equations (4.20).
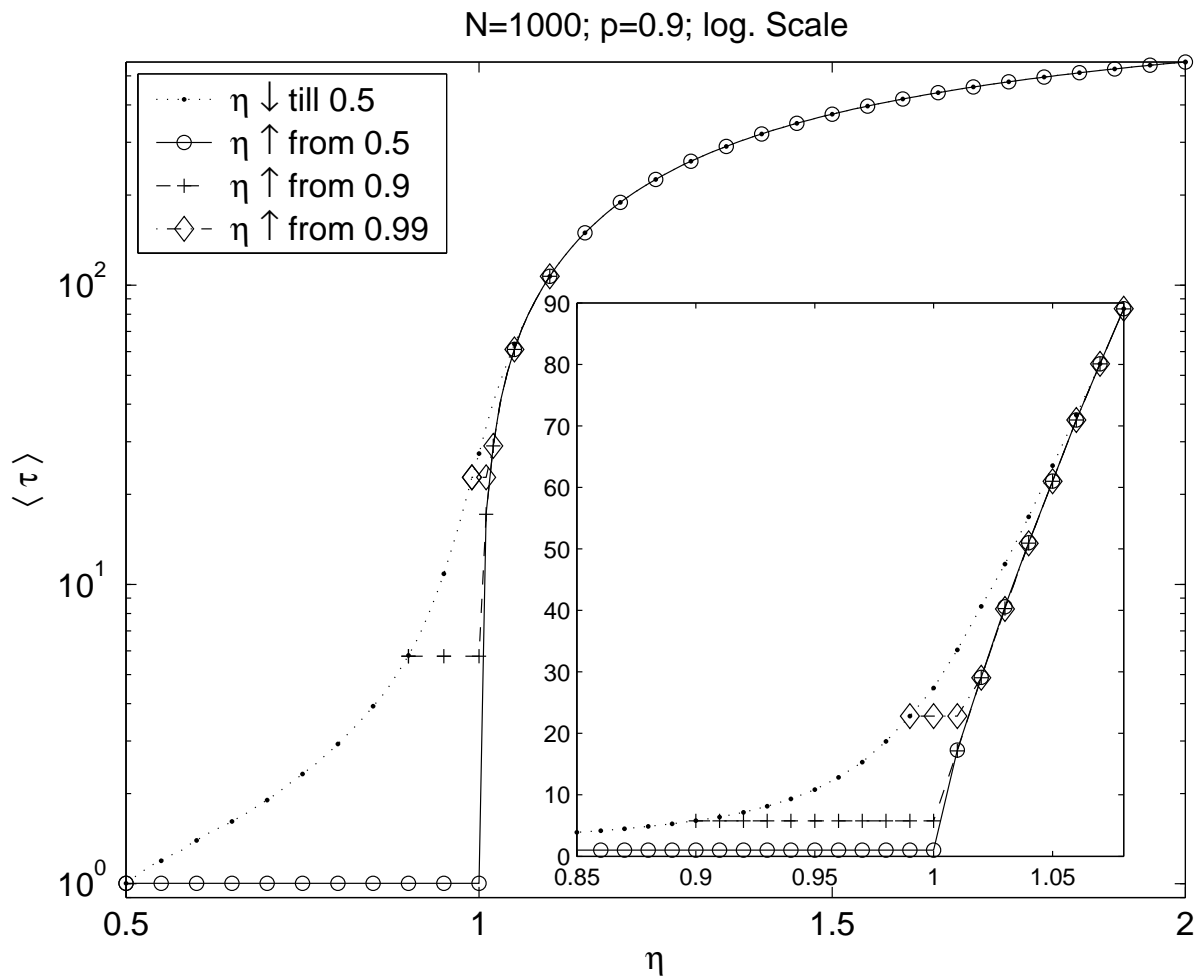
Figure 6: Hysteresis effect in the comparison of the dependence of $\langle \tau \rangle$ on η between the concentration and dilution process of the experiments. The y-axis shows $\langle \tau \rangle$ of 1000 experiments in logarithmic scale. Four curves are shown: $\eta \downarrow$ till 0.5: shows the results of the concentration process till $\eta = 0.5$. $\eta \uparrow$ from 0.5 is the corresponding part of 1000 dilution processes starting from $\eta = 0.5$. $\eta \downarrow$ from 0.9 shows the result for the dilution process starting after a concentration till $\eta = 0.9$. And $\eta \downarrow$ from 0.99 the same for a concentration until $\eta = 0.99$. The inset shows a zoom on the interesting region around $\eta = 1$ in linear scale. The number of neurons $N = 1000$ equals threshold L and $p = 0.9$ in all cases.

After an initial transient the deterministic system shows a periodic pattern of spikes. The period of a pattern is the ISI of the ensemble (Figure 1b and 1c illustrate such patterns). If we take an arbitrary neuron and start the pattern at a spike of this unit, all units will spike exactly once until the next spike of the same unit. The sequence of these spikes will then start again with exactly the same time differences between the spikes, and this pattern will repeat itself forevermore if the parameters of the system are not changed. One can derive the following condition the system fulfills if it shows a periodic firing pattern.

Periodic pattern condition. *A system that consists of κ clusters, where every cluster i consists of k_i elements, shows a periodic firing pattern with ISI τ if for every $i \in \{1, \ldots, \kappa\}$*

$$k_i > k_{min}(\tau) = \begin{cases} (N-1)(1-\eta) + \frac{p(\tau-1-t_{ref})}{\epsilon} & \text{if } \tau \geq 1 + t_{ref} \\ (N-1)(1-\eta) & \text{if } \tau < 1 + t_{ref} \end{cases} \quad (4.4)$$

is fulfilled.

For derivation of this rule see Appendix A. Condition (4.4) simply tells us that every cluster (i.e. units that reach the threshold at the same time-step) has to be greater than a certain minimum cluster size which depends on the system's parameter and its ISI.

Before we continue our analysis we make some comments on the validity of this rule for the stochastic system. The firing patterns of the deterministic system may also occur in the stochastic system as can be seen in Figure 1b and 1c. According to the robustness of these patterns against variations in the stochastic evolution we can distinguish between three types of patterns.

Robust firing patterns are totally insensitive to variations of stochastic state transitions in the sense that, no matter how they evolve, even if they are totally suppressed, the system cannot change its periodic pattern.

Semi-robust firing patterns remain unchanged if one or more units evolve slower than with their mean velocity p, but if they evolve much faster the spiking pattern may change. Since such changes are rare, as will be explained subsequently, and the patterns are robust against at least half of the possible stochastic events, we choose the name semi-robust.

Variable firing patterns may change due to very slow or very fast evolution of one or more units.

At $\eta \leq 1$ we can find only robust and semi-robust patterns. Condition (4.4) gives us the rule for a semi-robust pattern in the stochastic system. To get the condition of a robust pattern in this case we would have to replace p with 1.

A change of a semi-robust pattern of phase-locked clusters implies that one or more units change from one cluster to the one firing directly before it. This increases the robustness of the resulting new firing pattern since the smallest cluster has the highest probability of receiving a neuron and leads to a certain balancing of the sizes of the clusters. Only if we have two small clusters spiking one directly after the other a merge of these two clusters might occur, which would imply a decrease of the ISI. Every decrease of the ISI enhances the robustness of the resulting firing pattern, since it implies a decrease of the minimum cluster size $k_{min}(\tau)$. Such events however are rare especially for large populations and their influence is far below the standard deviation of the experiments. Since we are mainly interested in the ISIs of our system we can neglect them in our analysis. Although we have to state that for an infinite simulation time all semi-robust patterns would transform into robust ones.

For $\eta > 1$ we only find variable firing patterns (Figure 1a). In the stochastic system, the higher the value of η the lower is the probability to observe between three consecutive spikes of a certain single unit the same two spiking patterns of the rest of the neurons. It is not even granted that the two ISIs of this unit have the same length. But now, unlike the case of $\eta \leq 1$, the fluctuations of the noise cannot create irreversible effects on the ISI of the system. The mean ISI of the system coincides therefore with the one of the deterministic system, which makes the following analysis valid in this region as well.

Every time the coupling strength is increased, after a short transient, the deterministic system fulfills again condition (4.4). This allows us to make some observations on the ISI of the system. Since the cluster sizes have to be integer numbers we define

$$\hat{k}_{min}(\tau) = \lfloor k_{min}(\tau) + 1 \rfloor \tag{4.5}$$

and have the condition $k_i \geq \hat{k}_{min}(\tau)$. This definition guarantees that $\hat{k}_{min}(\tau) \geq 0$ and is necessary for technical reasons in the derivation of the lower bound we will see later. A

system with ISI τ consists of $\kappa = \tau/\delta$ clusters since a spiking cluster at time t provokes the spiking of the next one at time $t + \delta$. With this we calculate another quantity we need to describe our system, the mean cluster size given a certain ISI τ:

$$\bar{k}(\tau) = \frac{N\delta}{\tau} \ . \tag{4.6}$$

We then introduce a new function $g(\tau)$ which gives us the ratio between $\bar{k}(\tau)$ and $\hat{k}_{min}(\tau)$.

$$g(\tau) = \frac{\bar{k}(\tau)}{\hat{k}_{min}(\tau)} \ . \tag{4.7}$$

Intuitively this quantity can be seen as the frequency a system consisting only of clusters with the minimum cluster size $\hat{k}_{min}(\tau)$ has to fire with, to achieve the same ISI as the system with cluster-size $\bar{k}(\tau)$. Note that $g(\tau) > 0$ since $\hat{k}_{min}(\tau) \geq 0$.

Using equation (4.5) of the minimum integer cluster size $\hat{k}_{min}(\tau)$ we arrive after some manipulation to the following inequality (See equation (B.15) in Appendix B for details).

$$\frac{N\delta}{\langle\tau\rangle} \leq \langle g \rangle \left(k_{min}(\langle\tau\rangle) + 1 \right). \tag{4.8}$$

$\langle g \rangle$ denotes the expectation of $g(\tau)$ with respect to the probability distribution of τ. We will call $\langle g \rangle_{min}$ from now on the minimum value, which $\langle g \rangle$ can take to fulfill inequality (4.8). Using $\langle g \rangle_{min}$ inequality (4.8) can be written as

$$\frac{1}{\langle\tau\rangle} = \langle g \rangle_{min}\zeta \ , \tag{4.9}$$

when we replace $(k_{min}(\langle\tau\rangle) + 1)/(N\delta)$ with ζ. If we plot $\langle\tau\rangle$ and ζ in double logarithmic scale we notice a nearly linear dependence between $1/\langle\tau\rangle$ and ζ. This is the reason why by replacing $\langle g \rangle_{min}$ with a constant one can get a good approximation of $\langle\tau\rangle$ as we will see later. Two examples for this nearly linear relation can be seen in Figure 7a for noise rates of $p = 0.9$ and $p = 0.6$. The inset shows a comparison between ζ and η for $p = 0.9$. If we take a closer look on $\langle g \rangle_{min}$ however, we notice that the hypothesis of a linear relationship does not hold. In Figure 7b we can observe the exact value of $\langle g \rangle_{min}$ for the corresponding two sets of experiments. From empirical evidence we can suppose, that for the values of p and η of our simulations 2 is an upper bound of $\langle g \rangle_{min}$, which allows us to replace $\langle g \rangle$ with 2 in inequality (4.8).

4.3.1 Bounds for τ and $\langle\tau\rangle$

With the results of the last section we can derive upper and lower bounds for τ and the mean ISI $\langle\tau\rangle$. Both bounds of $\langle\tau\rangle$ can be used to approximate $\langle\tau\rangle$.

First we derive a lower bound for $\langle\tau\rangle$ using definition (4.7) and condition (4.8). [4]

$$\langle\tau\rangle_{min} = \frac{(N-1)\epsilon(\eta-1) - \epsilon}{2p} + \frac{1 + t_{ref}}{2} + \sqrt{\left(\frac{(N-1)\epsilon(\eta-1) - \epsilon}{2p} + \frac{1 + t_{ref}}{2}\right)^2 + \frac{N\epsilon\delta}{p\langle g\rangle}} \tag{4.10}$$

In the following we will use (if not stated differently) the empirical upper bound 2 of $\langle g \rangle_{min}$ as explained in the previous section to substitute $\langle g \rangle$ in (4.10) and to calculate the

---

[4]Note that if $\langle g \rangle$ is replaced by $\langle g \rangle_{min}$ in (4.10) we get an expression for $\langle\tau\rangle$.

numerical values of $\langle\tau\rangle_{min}$.

To get an upper bound for all possible ISIs we use (4.4) and (4.6):

$$\tau_{max} = \frac{(N-1)\epsilon(\eta-1)}{2p} + \frac{1+t_{ref}}{2} + \sqrt{\left(\frac{(N-1)\epsilon(\eta-1)}{2p} + \frac{1+t_{ref}}{2}\right)^2 + \frac{N\epsilon\delta}{p}} \quad (4.11)$$

and have that (See Appendix B for details):

$$\langle\tau\rangle_{min} \leq \langle\tau\rangle \leq \tau_{max} . \quad (4.12)$$

Note that τ_{max} is an upper bound for all ISIs τ whereas $\langle\tau\rangle_{min}$ is only a lower bound for $\langle\tau\rangle$ but not for τ. Because of this fact $\langle\tau\rangle_{min}$ is much closer to $\langle\tau\rangle$ than τ_{max}, as we can observe in the Figures 7c and 7d which show the quality of these bounds. The solid line in Figure 7c represents $\langle\tau\rangle$ for 1000 concentration processes in logarithmic scale. It lies within a gray area that indicates the interval limited by the two bounds $\langle\tau\rangle_{min}$ and τ_{max}.
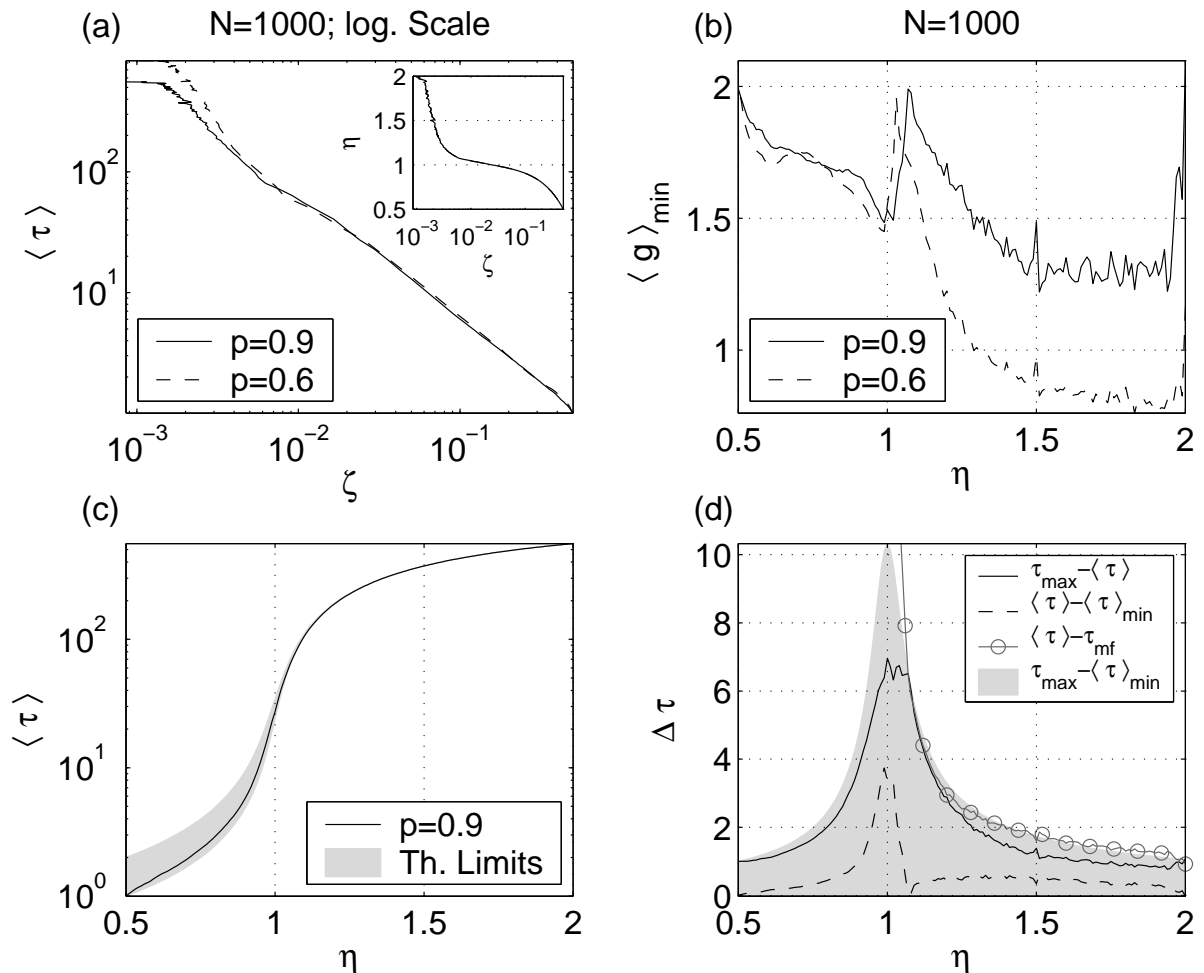

Figure 7: **(a)** Relation of $\langle\tau\rangle$ and $\zeta = (k_{min}(\langle\tau\rangle) + 1)/(N\delta)$ for two different values of p. **(b)** Dependence of parameter $\langle g\rangle_{min}$ on η for two different values of p. We can observe $\langle g\rangle_{min} \leq 2$. **(c)** The empirical outcome $\langle\tau\rangle$ of the concentration processes of 1000 experiments compared to its theoretical limits τ_{max} and $\langle\tau\rangle_{min}$ (gray area). **(d)** Difference between the theoretical limits τ_{max} and $\langle\tau\rangle_{min}$ (gray area), $\langle\tau\rangle$ and $\langle\tau\rangle_{min}$ (dashed line), τ_{max} and $\langle\tau\rangle$ (black solid line), $\langle\tau\rangle$ and τ_{mf} (gray solid line with circles). τ_{max} has been calculated using equation (4.11) and $\langle\tau\rangle_{min}$ substituting 2 for $\langle g\rangle$ in equation (4.10).

In Appendix B.2 we derive a lower bound $\tau_{min} \leq \tau$. $\tau_{min} = t_{ref}$ for $\eta < 1$ and coincides with the approximation τ_{mf} (see equation (2.5)) for $\eta \geq 1$. We have therefore that

$$\tau_{mf} \leq \tau \leq \tau_{max}. \tag{4.13}$$

The exact difference between $\langle \tau \rangle$ and its bounds is shown in Figure 7d. The difference $\langle \tau \rangle - \langle \tau \rangle_{min}$ is indicated by the dashed line, and $\tau_{max} - \langle \tau \rangle$ by the solid line. The gray area shows the width of the interval bounded by $\langle \tau \rangle_{min}$ and τ_{max}. The quantity $\langle \tau \rangle_{min}$ is, for a wide range of values of η, not only a bound but an excellent approximation for $\langle \tau \rangle$. It beats by far the approximation τ_{mf}, whose difference to $\langle \tau \rangle$ is shown by the gray solid line with circles in Figure 7d. In spite of this fact the importance of $\langle \tau \rangle_{min}$ and τ_{max} does not only lie in their quality as approximations, but rather in the fact that they are bounds and both experience a similar phase transition effect as $\langle \tau \rangle$. This allows us to derive the thermodynamic limit of $\langle \tau \rangle$.

4.3.2 Thermodynamic Limit

The thermodynamic limits (i.e. the behavior for infinite N and L and finite η) of the bounds from equation (4.10) and (4.11) can be derived after some calculations (See Appendix C for details) and allow to set bounds for the thermodynamic limit of $\langle \tau \rangle$.

$$
\begin{aligned}
&\lim_{N \to \infty} \langle \tau \rangle = \delta && \text{if } \eta < 0.5 \ , \\
&\frac{\delta}{\langle g \rangle (1 - \eta)} \leq \lim_{N \to \infty} \langle \tau \rangle \leq \frac{\delta}{(1 - \eta)} && \text{if } 0.5 \leq \eta < 1 \ , \\
&\sqrt{\frac{\epsilon \delta}{p \langle g \rangle}} \leq \lim_{N \to \infty} \frac{\langle \tau \rangle}{\sqrt{N}} \leq \sqrt{\frac{\epsilon \delta}{p}} && \text{if } \eta = 1 \ , \\
&\lim_{N \to \infty} \frac{\langle \tau \rangle}{N} = \frac{\epsilon(\eta - 1)}{p} && \text{if } \eta > 1 \ .
\end{aligned}
\tag{4.14}
$$

The upper bound at $0.5 \leq \eta < 1$ coincides with the one obtained for a model without stochastic input similar to (van Vreeswijk & Abbott, 1993). To characterize the quality of these bounds we examine the quantity $\Delta \tau = \tau_{max} - \langle \tau \rangle_{min}$, especially at its thermodynamic limit. The gray area in Figure 7d shows $\Delta \tau$ for the case of $N = 1000$ and $p = 0.9$. From (4.10) and (4.11) we can derive after some algebra that

$$
\lim_{N \to \infty} \Delta \tau =
\begin{cases}
0 & \text{for } \eta < 0.5 \ , \\[2mm]
\dfrac{\delta}{1 - \eta}\left(1 - \dfrac{1}{\langle g \rangle}\right) & \text{for } 0.5 \leq \eta < 1 \ , \\[3mm]
\displaystyle \lim_{N \to \infty}\left(1 - \dfrac{1}{\sqrt{\langle g \rangle}}\right)\sqrt{\dfrac{N \epsilon \delta}{p}} & \text{for } \eta = 1 \ , \\[3mm]
\dfrac{\epsilon}{p} + \dfrac{\delta}{\eta - 1}\left(1 - \dfrac{1}{\langle g \rangle}\right) & \text{for } \eta > 1 \ .
\end{cases}
\tag{4.15}
$$

Since from $\tau_{max} \geq \langle \tau \rangle_{min}$ follows $\Delta \tau \geq 0$, we have that $\langle g \rangle$ and $\langle g \rangle_{min}$ have lower bounds:

$$
\lim_{N \to \infty} \langle g \rangle \geq \lim_{N \to \infty} \langle g \rangle_{min} \geq
\begin{cases}
1 & \text{for } \eta \leq 1 \ , \\[2mm]
\dfrac{p\delta}{p\delta + (\eta - 1)\epsilon} & \text{for } \eta > 1 \ .
\end{cases}
\tag{4.16}
$$

If we compare $\Delta\tau$ with the difference of τ_{mf} and τ_{max} we get

$$\lim_{N\to\infty} (\tau_{max} - \tau_{mf}) = 1 + \frac{\delta}{\eta - 1} \quad \text{for } \eta > 1 . \tag{4.17}$$

For high values of η the limit of this difference tends to 1. Therefore the formulas (2.5) of Rodríguez et al. (2001) really represent a good approximation of the dynamics for $\eta \gg 1$.

Approximation with $\langle\tau\rangle_{min}$ however is always closer to $\langle\tau\rangle$ if $p \geq \epsilon$. In the case of $p < \epsilon$ we can derive using $\langle\tau\rangle \geq \tau_{mf}$ an upper bound for $\langle g\rangle_{min}$.

$$\lim_{N\to\infty} \langle g\rangle_{min} \leq \frac{p\delta}{(\eta - 1)(\epsilon - p)} \quad \text{if } \eta > 1 \text{ and } p < \epsilon . \tag{4.18}$$

As long as we use a value lower than the right hand side of inequality (4.18) to replace $\langle g\rangle$ in (4.10), the approximation of $\langle\tau\rangle$ with $\langle\tau\rangle_{min}$ beats τ_{mf} also for $\eta > 1$ and $p < \epsilon$, and is therefore an improvement to earlier studies for all values of η.

4.3.3 Application of the Thermodynamic Limit

If we suppose a dependence of $\langle\tau\rangle$ on N as in (4.1) ($\alpha N^c \sim \langle\tau\rangle$) we can now derive the thermodynamic limits for α and c from the above results. See appendix C for details. The value of c is rather straightforward.

$$\lim_{N\to\infty} c = \begin{cases} 0 & \text{for } \eta < 1 , \\ 0.5 & \text{for } \eta = 1 , \\ 1 & \text{for } \eta > 1 . \end{cases} \tag{4.19}$$

This observation coincides with the experimental results presented in Figure 4 and indicates a linear dependence between the ISI and the number of neurons N for $\eta > 1$, whereas for $\eta < 1$ the ISI does not depend on the amount of units in the ensemble at all. In between at $\eta = 1$ the mean value of the ISI distribution $\langle\tau\rangle$ depends on $\sqrt{N}$.

The thermodynamic limit of α follows straightforward from (4.14). We get:

$$\lim_{N\to\infty} \alpha = \delta \qquad\qquad \text{if } \eta < 0.5 ,$$

$$\frac{\delta}{\langle g\rangle(1-\eta)} \leq \lim_{N\to\infty} \alpha \leq \frac{\delta}{(1-\eta)} \qquad \text{if } 0.5 \leq \eta < 1 ,$$

$$\sqrt{\frac{\epsilon\delta}{p\langle g\rangle}} \leq \lim_{N\to\infty} \alpha \leq \sqrt{\frac{\epsilon\delta}{p}} \qquad \text{if } \eta = 1 ,$$

$$\lim_{N\to\infty} \alpha = \frac{\epsilon(\eta - 1)}{p} \qquad\qquad \text{if } \eta > 1 . \tag{4.20}$$

Since we can replace $\langle g\rangle$ with $\langle g\rangle_{min}$ and $1 \leq \langle g\rangle_{min} \leq 2$ for $\eta \leq 1$ we get an excellent approximation for α at the limit of large N. We can observe this in Figure 5. The shaded area shows the possible regions of α. Already for low N the experimental data fits well into the theoretical results for the thermodynamic limit, which give an idea what ISI to expect for $\eta < 1$.

4.3.4 Hysteresis

Condition (4.4) for a periodic spiking pattern gives us also the explanation of the hysteresis phenomena. In the dilution process we always start from a robust or semi-robust pattern at $\eta \leq 1$ and condition (4.4) is not altered by an increase of η. The inequality gets even

sharper, which means that the probability of changing a semi-robust pattern is even lower the more we increase η. In other words: the semi-robust patterns tend to be robust during the dilution process. This changes once we reach $\eta = 1$, since now the stochastic state transitions are needed again to maintain the ISIs. But even for $\eta > 1$ the ISI may remain constant as long as the following condition is fulfilled. (See Appendix B.2 for details and derivation)

$$\tau \geq t_{ref} + \frac{(N-1)\epsilon(\eta-1)}{p} \ . \tag{4.21}$$

This inequality reflects that the approximations (2.5) of Rodríguez et al. (2001) are a lower bound for the ISI in the dilution process, which have to be fulfilled by the deterministic system. Only when a value of η violating this condition is reached, the system leaves the ISI it has fired with since the beginning of the dilution process and changes to a new ISI which does fulfill the condition. We can observe this in the dashed-dotted line with $\diamond$ markers of Figure 6 which shows a dilution process started already at $\eta = 0.99$. In this case $\langle \tau \rangle$ remains constant even for $\eta = 1.01$ since inequality (4.21) is still fulfilled at this point. Only if we dilute further $\langle \tau \rangle$ increases to values fulfilling condition (4.21) and starts to coincide with $\langle \tau \rangle$ of the other two dilution processes. Approximately at $\eta = 1.08$ the mean ISI of dilution processes coincides with the one of the concentration processes, since then the equations (2.5) start to approximate $\langle \tau \rangle$ well again.

5 Heterogeneous networks

In this section we show that the results described in section 4 for homogeneous networks can be extended to networks consisting of neurons with heterogeneous coupling strengths and thresholds.

5.1 Generalization of the model

To be able to simulate heterogeneous networks we have to apply the following extensions to the model presented in section 2.

- Instead of setting all coupling strengths ϵ_{ij} equal to an homogeneous coupling strength ϵ we take the ϵ_{ij} from a Gaussian distribution with mean $\langle \epsilon \rangle$.

- We allow heterogeneous thresholds L_i for every unit. Each L_i is taken form a Gaussian distribution with mean $\langle L \rangle$.

- The relation (denominated s) between standard deviations and means of both distributions is fixed.

- To characterize the new extended system we calculate the parameter η in the same way as before but use the mean values $\langle \epsilon \rangle$ and $\langle L \rangle$ of the distributions instead of L and ϵ of a homogeneous network. We call this parameter η_{ext}.

$$\eta_{ext} = \frac{\langle L \rangle - 1}{(N-1)\langle \epsilon \rangle} \ . \tag{5.1}$$

With this model of a heterogeneous network we perform the same type of experiments as described in section 3. In the concentration process we start in regions with high η_{ext} and increase the connection strengths of the system adiabatically. As in the experiments with homogeneous networks we increase it by resting a constant value $\Delta\eta_{ext}$ from η_{ext}. We have to calculate the corresponding values of ϵ_{ij} after the change by multiplying them by $\eta_{ext}/(\eta_{ext} - \Delta\eta_{ext})$. Thus we achieve that after every change equation (5.1) is still valid.

5.2 Results for heterogeneous networks

We compare experiments with the generalized model with the results of section 4 for homogeneous networks. Figure 8 shows this comparison for the values of α (Figure 8a) and c (Figure 8b) of equation (4.1).

The only noticeable difference between experiments with homogeneous networks (solid black line) and the corresponding heterogeneous equivalents with deviations of 10% (dash-dotted line) and 30% of the mean value (gray solid line with circles)

is that for $\eta \leq 1$ the curves show some irregular bumps which differ from the expected
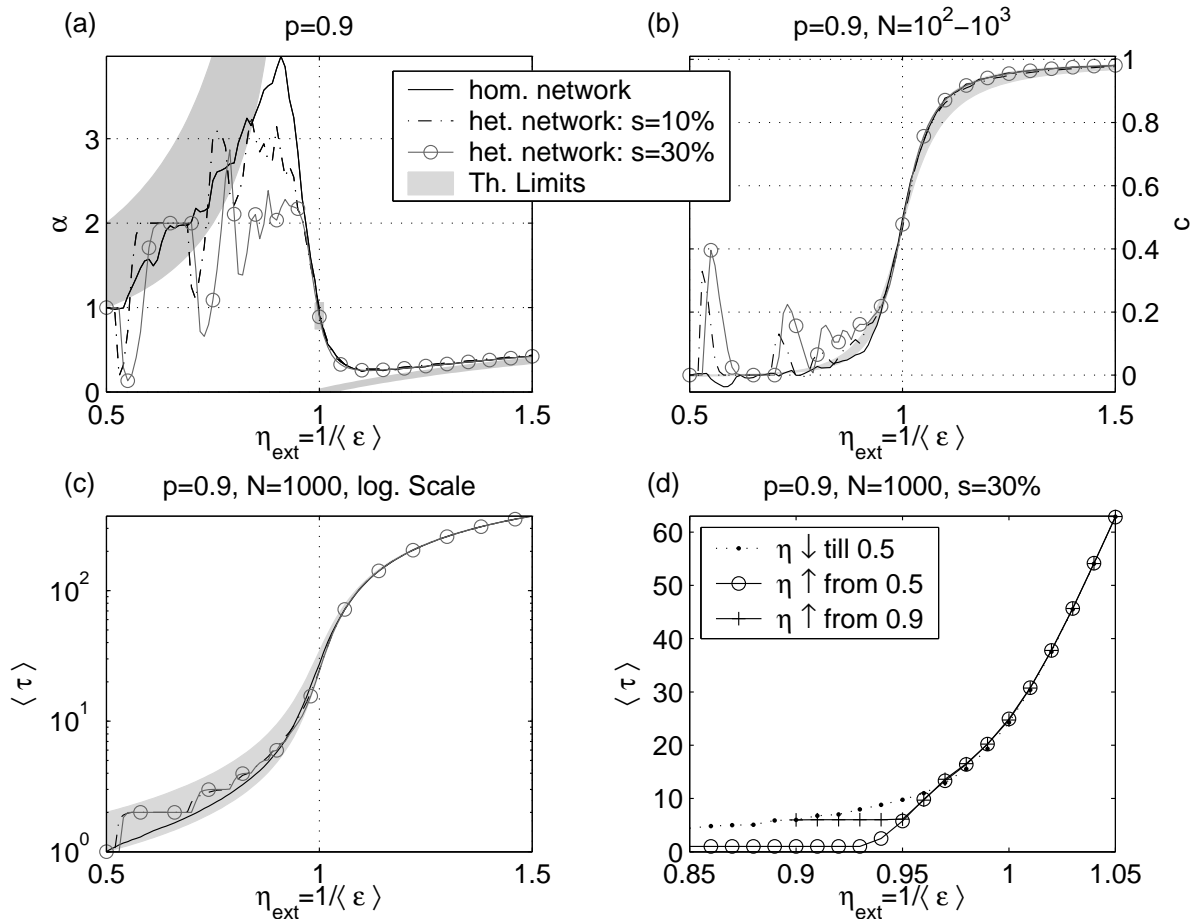

Figure 8: **(a)**, **(b)** and **(c)** compare the results of 1000 experiments with homogeneous and heterogeneous networks. **(a)** shows α and **(b)** c under the assumption that $\langle \tau \rangle = \alpha N^c$ for $N \in \{100, 200, \ldots 1000\}$. Coupling strengths and thresholds where taken from Gaussian distributions with deviations of 10% (dash-dotted line) and 30% (gray solid line with circles) of their means. The black solid lines (homogeneous network) coincide with the results shown in Figures 4 and 5, as well as the the shaded areas, which represent in **(a)** the regions of possible values of α for $N \to \infty$ according to equations (4.20) and in **(b)** the region of possible values of c obtained using equations (4.10) and (4.11) for finite N as in the experiments. **(c)** Comparison only of the results for $N = 1000$. The mean ISIs $\langle \tau \rangle$ of the heterogeneous experiments lie within the gray area bounded by $\langle \tau \rangle_{min}$ (Eq. (4.10)) and τ_{max} (Eq. (4.11)). Compare with Figure 7c. We notice that the results obtained for the theoretical bounds of the ISI are also valid for heterogeneous networks. **(d)** Hysteresis in a heterogeneous network with $s = 30\%$. Compare with Figure 6. Hysteresis does also occur in heterogeneous networks, but vanishes there already at η slightly lower than 1.

values (gray areas) of the theoretical analysis. A closer examination of the ISIs at $\eta < 1$ reveals that this bumps are provoked by jumps between integer values of the ISI, as can be observed in Figure 8c, which shows $\langle \tau \rangle$ for $N = 1000$. Contrary to intuition the smooth change of the mean ISI in the homogeneous case (black solid line) is more step-like in heterogeneous networks, meaning that for certain intervals of the coupling strength (i.e. the plateaus in Figure 8c) nearly all the experiments (with different networks) end up with the same ISI. The observed behavior, which is reproducible and robust despite the stochastic inputs and the heterogeneity of the network, is not fully understood, but might be of biological relevance and will be subject of future research. The locations of the steps depend on the ensemble size N, which causes the bumps in Figures 8a and 8b. In the thermodynamic limit, however, these bumps should disappear.

In spite of this effect, the upper and lower bounds for $\langle \tau \rangle$, given by equations (4.10) and(4.11) and represented by the gray area in Figure 8c, are valid even for high deviations of the underlying probability distributions. Also the hysteresis effect is present in the heterogeneous networks (Figure 8d), although it vanishes slightly before the critical coupling strength is reached at $\eta = 1$ (compare with Figure 6). This is caused by some neurons which receive less input compared with their threshold than the others. They need stochastic input to reach the threshold already slightly below $\eta = 1$, which can cause the end of self-sustained firing and an increase in the ISI of the ensemble.

6 Sequential versus Parallel Dynamics

The results presented so far have been obtained using parallel updating of the units, meaning that at every time-step all units are updated. Sometimes sequential dynamics, where only a reduced number of neurons is updated at every time-step, are used to simulate neural dynamics instead (Herz & Marcus, 1993). It has been shown that sequential and parallel updating can lead to different behavior of the Hopfield model (Fontanari & Köberle, 1988) and multi-state Ising-type ferromagnets (Bolle & Blanco, 2004), which motivates us to investigate the dependence of our results on the type of updating. We will use the most simplest case of sequential updating, where only one neuron is updated at each time-step and modify the model presented in section 2 in the following way:

- One time-step of the original model is split up into N time-steps and at each new time-step only one neuron is updated. A specific neuron i is updated at every time-step t which fulfills $i \equiv t \mod N$.

- Given a synaptic delay δ^{seq} and a refractory period t_{ref}^{seq}, the neuron which is updated at time t receives all the spikes which have been sent within the interval $[t - N - \delta^{seq}, t - \delta^{seq})$ by the other neurons. In the case that neuron i made spike in the last time-step, the interval narrows to $[t - N - \delta^{seq} + t_{ref}^{seq}, t - \delta^{seq})$.

This modification implies that the synaptic delay is no longer homogeneous. An update of a post-synaptic unit occurs now the next time it is updated instead of the precise time-step when the spike would reach the unit. Therefore the effective delay is uniformly distributed between δ^{seq} and $\delta^{seq} + N$, leading to an average delay of

$$\langle \delta^{seq} \rangle = \delta^{seq} + N/2. \tag{6.1}$$

To compare simulations with sequential and parallel dynamics we have to set δ^{seq} accordingly to fulfill $N\delta = \langle \delta^{seq} \rangle$ where δ is the delay of the parallel dynamics. This leads to

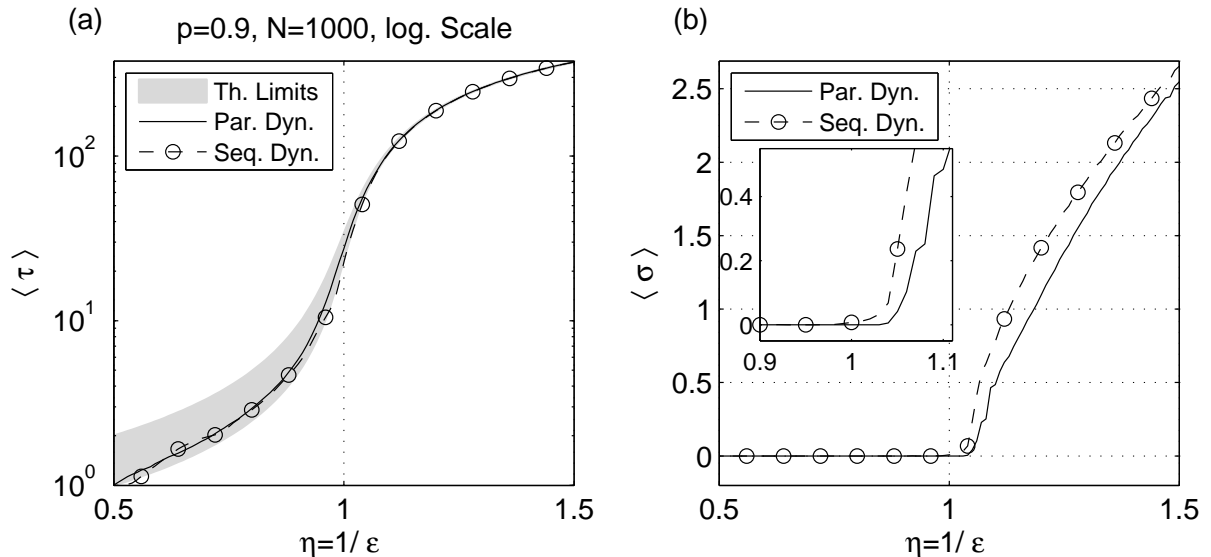$$\delta^{seq} = N \left(\delta - \frac{1}{2} \right). \tag{6.2}$$

Figure 9: Comparison of 1000 experiments with parallel dynamics (continuous lines) and their equivalent with sequential updating (dashed lines with circles). Number of neurons $N = 1000$ equals threshold L and $p = 0.9$. The results for the sequential dynamics are rescaled by the factor 1000. **(a)** The mean ISIs $\langle \tau \rangle$ of both type of dynamics nearly coincide and lie within the gray area bounded by $\langle \tau \rangle_{min}$ (Eq. (4.10)) and τ_{max} (Eq. (4.11)). **(b)** The sequential dynamics show a slightly higher mean of deviation $\langle \sigma \rangle$ of the units ISIs with the same experiments as the parallel dynamics for $\eta \geq 1$ but also end up in phase-locked clusters at $\eta < 1$. The inset shows a zoom on the interesting region around $\eta = 1$.

The equations for upper (Eq. (4.11)) and lower bounds (Eq. (4.10)) obtained for the parallel dynamics are valid only if $t_{ref} \leq \delta$, which means that the only noticeable effect of t_{ref} on the ensemble dynamics is that the threshold L acts as an absorbing barrier. To achieve the same effect in the sequential model we have to set $t_{ref}^{seq} = 1$. A greater t_{ref}^{seq} would lead to absorption of more spikes than in the corresponding parallel experiments and in consequence a greater ISI of the ensemble.

If we consider these two constraints we obtain similar results for both type of dynamics, as shown in Figure 9, where we compare simulations with increasing coupling strength for $N = 1000$ neurons and a noise rate $p = 0.9$. Since the delay δ of the parallel simulations equals 1, δ^{seq} was set to 500. This implies a mean delay $\langle \delta^{seq} \rangle$ of N, which is coherent with the rescaling of t to t/N. We observe in Figure 9a that after rescaling (i.e. dividing the ISI by the ensemble size) the mean ISI of the sequential dynamics (dashed line with circles) nearly coincides with the result of the parallel simulations (continuous line), and the bounds obtained in section 4.3 are valid also for this type of dynamics. Hysteresis can also be observed (data not shown). Units with sequential updating show due to the inhomogeneous delays a slightly greater deviation of their ISIs than their equivalents with parallel updating (see Figure 9b). This effect causes that phase-locked clusters, although observable also at $\eta = 1$, appear as a general phenomena (i.e. $\langle \sigma \rangle = 0$) for couplings slightly greater than the critical coupling strength as we can observe in the inset of Figure 9b.

Despite these small differences due to the enhanced dispersion of the ISIs we can conclude that the results derived in the previous section are also valid if sequential instead of parallel updating is used.

7 Discussion

We analyzed, by varying its coupling strength ϵ, the behavior of an ensemble of stochastic, non-leaky integrate-and-fire neurons with delayed, excitatory global coupling and a small refractory period. Around a critical value of the coupling strength the behavior of the system undergoes a phase transition (Figure 4), which has three main consequences on the dynamics of the ensemble:

Transition from irregular to clustered spiking behavior: The units of the ensemble are homogeneous but show, due to a stochastic component in their evolution towards threshold, irregular spiking behavior if they are weakly coupled (Figure 1a). The coupling strength ϵ is inversely proportional to the parameter η (see equation (2.4)), which describes the system and allows to fixate the phase transition at $\eta = 1$. For coupling greater than or equal to the coupling at $\eta = 1$ the population splits into several clusters. All neurons within a cluster spike in unison, although they still might show different trajectories towards the threshold. The clusters are phase-locked (Figure 1b) and have all exactly the same ISI, which is proportional to the number of clusters. This number decreases if the coupling is increased further (Figure 1c), but usually remains greater than 1 until a trivial case of only one cluster is reached at latest at $\eta < 0.5$. The activity at $\eta \leq 1$ is self-sustained in the sense that the stochastic inputs are not needed to maintain the clustered spiking activity.

Hysteresis: The phase transition is accompanied by a hysteresis effect (Figure 6). We applied a cyclic process to our system which consisted of two subprocesses: a concentration process where we increased ϵ and a dilution process where ϵ is decreased. Starting at an initial configuration with low coupling the process is reversible as long as we do not reach (at values of η slightly greater than 1) the onset of phase-locking. If we increase the coupling strength further the ISI τ of the concentration process decreases following rules explained below, whereas if we inverse the process (start the dilution process) the ISI remains frozen as long as $\eta \leq 1$. Then it jumps up to a value fulfilling condition (4.21) and coincides again with the ISI of the concentration process at η slightly greater than 1.

Change in the dependence of the ISI on ensemble size and noise rate: For low coupling the mean ISI $\langle \tau \rangle$ of the ensemble in the concentration process depends linearly on the ensemble size N, at $\eta = 1$ there is a square root dependence on N, whereas for coupling greater than at $\eta = 1$ the mean ISI $\langle \tau \rangle$ does not depend on N nor on the rate of the stochastic component, which governs the dynamics for low coupling. Between $\eta = 1$ and $\eta = 0.5$ the ISI only depends on the coupling strength itself. For a coupling greater than at $\eta = 0.5$ the influence of ϵ on the ISI is also lost. The length of the time delay determines the length of the ISI in this regime.

To obtain analytical results we used a deterministic approach to the model dynamics which allowed us, using a simple condition (4.4), to derive upper and lower bounds (τ_{max} and $\langle \tau \rangle_{min}$) for the mean ISI $\langle \tau \rangle$ of the ensemble in the concentration process. The lower bound $\langle \tau \rangle_{min}$ is also an excellent approximation for $\langle \tau \rangle$, as can be observed in Figure 7d. Using the bounds we can calculate the behavior of the system at its thermodynamic limit (i.e. for $N \to \infty$) and characterize the phase transition analytically.

These theoretical results are also valid if sequential instead of parallel updating (Herz & Marcus, 1993) is used to simulate the dynamics (Figure 9). In this case the synaptic delay is no longer homogeneous, leading to a slightly higher deviation of the unit's ISIs

and in consequence a slightly later onset of clustered spiking behavior in the concentration process.

The above explained effects could also be observed if, instead of an increase or decrease of the coupling strength, positive or negative external input were be added to the system. To calculate the critical point in this case we would have to add the external input to the denominator of equation (2.4) to get the appropriate value of η.

Using the hysteresis effect one can generate a simple memory by stimulating the system with a strong input, which leads the system to a value below $\eta = 1$. If the input is then substituted by a smaller one, which is just big enough to maintain the system below the critical couping strength and could represent the will to remember the first input, the ISI and the firing pattern of the ensemble will still be the same as if the strong input were still present. Once the system receives a short erase signal (e.g. in form of a negative input, or the absence of the small input), which allows it to reach a state corresponding to $\eta > 1$, the firing pattern produced by the strong input will disappear (i.e. the memory will be deleted). Such a mechanism might be a novel way to represent working memory functions (Wang, 2001), which are often modeled in the form of bistable dynamical attractor networks (Durstewitz et al., 2000). In our case it seems that we have multi-stability for coupling greater than the critical coupling strength, but further analysis is needed to verify this claim.

The main difference of our model to those used in earlier studies is the use of discrete time dynamics and that we combine delayed coupling with an implicit refractory period. Setting delay δ and refractory period t_{ref} identical and equal to 1 in the experiments does not represent a critical restriction on the presented results as can be seen in the theoretical analysis, which is valid in the general case as long as $\delta \geq t_{ref}$ and both are positive. We can observe as well from equations (4.15) and (4.17) that in a system with no delay, i.e. $\delta = 0$, the upper and lower bounds nearly coincide, leaving no space for clustering with more than one cluster and hysteresis. For a delay lower than the refractory period some of the inter-population messages would get absorbed, leading to different upper and lower bounds for the ISIs. Such a pair of bounds has been calculated for a system without stochastic input in (van Vreeswijk & Abbott, 1993) for the case of δ slightly lower than t_{ref}. We expect those results to be valid for our system at $\eta < 1$ in the thermodynamic limit. In the case of sequential dynamics the condition $\delta \geq t_{ref}$ translates into setting the refractory period to a minimum value.

It is straightforward to transfer the discrete time dynamics onto the continuous domain replacing the stochastic state transitions with a continuous increase of the state variable. This leads to continuous oscillators similar to the ones analyzed by Senn and Urbanczik (2000), but with the add-ons of delayed coupling and refractory period, which are both crucial to observe the reported phase transition and clustering phenomena. One can even maintain the stochastic dynamics using a continuous extension of the ISI distribution of a single uncoupled unit, a negative binomial distribution in our case (Rodríguez et al., 2001). Two different possibilities for such an extension have been presented by Gómez et al. (2006), leading both to gamma distributions. The length of delay and refractory-period remain untouched by these extensions. An analysis of these models is object of current research using a novel event-driven modelling technique (Gómez et al., 2006) allowing to simulate such extended models (also with non-integer values for delay and refractory period) without precision errors and without determining the exact trajectories of the states of the units in the ensemble. The derived formulas for upper and lower bounds should, apart from some minor modifications, be valid in these extended systems as well.

For models with a leaky term (Mirollo & Strogatz, 1990) clustering phenomena have been reported by Ernst et al. (1998) if a delay is added, but these clusters turned out

to be unstable for excitatory coupling if noise was added to the coupling strength. We conjecture that this behavior would change if a positive refractory period were included in the system. During the refractory period the threshold acts as an absorbing barrier allowing the system a certain tolerance against noise which is the higher the greater the amount of absorption is. The fact that Ernst et al. (1998) reports stability for inhibition is a clear evidence for this conjecture, since the reset state is a reflecting barrier in their model, allowing to absorb noisy negative coupling. It would also be interesting to observe the effect of delay and refractory period for a model with a biological inspired phase response curve (PRC). For this type of PRC the existence of a phase transition in the case of one (Östborn, 2002) and two dimensional (Östborn et al., 2003) oscillator lattices has been reported.

Our study shows that synaptic delay changes significantly neural dynamics. It is crucial for the observed hysteresis effect and the appearance of several phase-locked clusters. Without it we would get a totally synchronized ensemble at the critical coupling strength. The lack of a leaky term makes our model biologically plausible only at the limit of high coupling where integration of synaptic inputs occurs over a time scale much shorter than the decay constant (Burkitt & Clark, 1999), which is exactly where we find the phase transition and hysteresis. We therefore conjecture that the phenomena described could be found as well in more complex, realistic neural models with delay. Even in a system with inhomogeneous delays we can find similar results as shown for the case of sequential dynamics, which demonstrates the robustness of the findings.

In a network consisting of heterogeneous neurons with different coupling strengths and thresholds drawn from Gaussian distributions the reported phenomena are also present (Figure 8). This may be of great importance if synaptic dynamics are added to the model. We conjecture that in this context, plasticity may act as a homeostatic mechanism to maintain the system in the regime around the critical coupling strength if it experiences perturbations. In the neighborhood of the critical state the system explores all possible clusters one after the other. Clusters that are phase-locked after crossing this point are then transient states and the system is ready to set in any of the phase-locked, periodic firing patterns as a reaction to an increase in the number of received messages. This could have potential applications in a wide range of engineering applications like image segmentation (Campbell et al., 1999; Rhouma & Frigui, 2001) or large scale sensor networks (Hong & Scaglione, 2005), where clustering might be useful to optimize the information throughput. The application of the results to information processing in natural systems is the subject of current research.

As a final aspect we would like to highlight the application of our model (interpreted as a network of pulse-coupled oscillators with stochastic frequencies) to describe animal behavior, e.g. populations of flashing fireflies (Buck, 1988). For the North American firefly several types of synchronization have been reported (Copeland & Moiseff, 1995) and it seems that a certain number of flashing flies within a certain area is needed to observe synchronization. This would be in consonance with our model, where an increase in the number of units (fireflies) would decrease the coupling parameter η. For a certain number of units we would reach the critical point, where synchronization would appear. Apart form unison synchrony, wave synchrony has been observed, which might be explained by the clusters we report.

Appendix A   Proof of Periodic Pattern Condition 4.4

In the following analysis we use the deterministic rule (4.3) instead of the stochastic state transitions (2.1) and restrict ourself to the case of $\delta \geq t_{ref}$. A unit with ISI τ can make

$\tau - 1 - t_{ref}$ transitions due to this rule before reaching the threshold. The term t_{ref} corresponds to the refractory period where no increase of the state of an unit is allowed and the -1 to the last time-step when the threshold is reached. We have therefore a contribution of $p(\tau - 1 - t_{ref})\Theta(\tau - 1 - t_{ref})$ because of rule (4.3) to the total evolution of a neuron before its threshold is reached[5].

With this result we can calculate the mean minimum cluster size of a system of κ clusters. We call the clusters K_i ($i \in \{1, \ldots, \kappa\}$) and set the number of elements of every cluster $|K_i| = k_i$. The clusters are ordered according to their spiking time. At every time-step one cluster reaches threshold starting with cluster K_1. After cluster K_κ spikes the cycle starts again with cluster K_1. When cluster K_i reaches threshold, the elements of cluster K_{i+1} (or of K_1 in case of $i = \kappa$) have received the inputs of all clusters except cluster K_i and an increase of $p(\tau - 1 - t_{ref})$ due to rule (4.3). This leads to the following condition:

$$1 + \left(-1 + \sum_{\substack{j=1 \\ j \neq i}}^{\kappa} k_j \right)\epsilon + p(\tau - 1 - t_{ref})\Theta(\tau - 1 - t_{ref}) < L. \tag{A.1}$$

Which due to $\sum_{j=1}^{\kappa} k_j = N$ is equivalent to

$$k_i > k_{min} = N - 1 + \frac{1 + p(\tau - 1 - t_{ref})\Theta(\tau - 1 - t_{ref}) - L}{\epsilon} \qquad \text{for all } i \in \{1, \ldots, \kappa\}. \tag{A.2}$$

Written in terms of η this is equal to

$$k_i > k_{min}(\tau) = (N-1)(1-\eta) + \frac{p(\tau - 1 - t_{ref})\Theta(\tau - 1 - t_{ref})}{\epsilon} . \tag{A.3}$$

We have proved the periodic pattern condition (4.4).

Appendix B Bounds for τ

In this appendix we derive bounds for the ISI τ of the ensemble and the mean ISI $\langle\tau\rangle$ of several experiments. Again we will use the deterministic rule (4.3) instead of the stochastic dynamics (2.1). We will obtain two absolute bounds such that $\tau_{min} \le \tau \le \tau_{max}$ for all possible ISIs of the system, and a lower bound for the mean value $\langle\tau\rangle$ over all possible initial conditions which we call $\langle\tau\rangle_{min}$. We get thus

$$\langle\tau\rangle_{min} \le \langle\tau\rangle \le \tau_{max} . \tag{B.1}$$

B.1 Maximum ISI τ_{max}

First we derive the maximum possible ISI τ_{max} of the system. It is obvious that the mean cluster size $\bar{k}(\tau) \ge k_{min}$, which can be written using equations (4.6) and (A.3) as

$$\bar{k}(\tau) = \frac{N\delta}{\tau} \ge (N-1)(1-\eta) + \frac{p(\tau - 1 - t_{ref})\Theta(\tau - 1 - t_{ref})}{\epsilon} . \tag{B.2}$$

This results in an inequality of degree 2 for τ which has the only solution

$$\tau \le \tau_{max} = \frac{(N-1)\epsilon(\eta-1)}{2p} + \frac{1+t_{ref}}{2} + \sqrt{\left(\frac{(N-1)\epsilon(\eta-1)}{2p} + \frac{1+t_{ref}}{2} \right)^2 + \frac{N\epsilon\delta}{p}} . \tag{B.3}$$

---

[5]Note the use of the Heaviside step function to have a valid formula also for the case of $\tau < t_{ref} + 1$.

compatible with the condition $\tau \geq 0$. We omitted the $\Theta(\tau - 1 - t_{ref})$ term to calculate (B.3). This can be done if $\tau \geq 1 + t_{ref}$. Inequality (B.2) permits us to calculate the minimum value of η for which a certain ISI τ is possible. We get

$$\eta \geq \eta_{min}(\tau) = \frac{p(\tau - 1 - t_{ref})\Theta(\tau - 1 - t_{ref})}{(N-1)\epsilon} + 1 - \frac{N\delta}{(N-1)\tau} \ . \tag{B.4}$$

It is sufficient to calculate $\eta_{min}(2\delta)$ since we assume that $\delta \geq t_{ref} \geq 1$ and the system will be fully synchronized ($\tau = \delta$), i.e. it consists of only one cluster, for values of η below this limit, which we call η_{sync}. We get

$$\eta \geq \eta_{sync} = 0.5 - \frac{1}{2(N-1)} + \frac{p(2\delta - 1 - t_{ref})\Theta(2\delta - 1 - t_{ref})}{(N-1)\epsilon} \ . \tag{B.5}$$

For the limit of large N this transforms into

$$\lim_{N \to \infty} \eta_{sync} = 0.5 \ . \tag{B.6}$$

Condition (B.3) is therefore valid if $\eta \geq 0.5$.

B.2 Minimum ISI τ_{min}

If, instead of looking at the state of a neuron before the threshold is reached as in the proof of the periodic pattern condition in appendix A, we observe the state of a neuron just after it has passed the threshold, we can derive a condition for the minimum possible ISI. We use that a neuron with an ISI of length τ increases its state due to the deterministic rule (4.3) by $p(\tau - t_{ref})$ during every ISI. Since all neurons are equal we expect that during an ISI of a single neuron every other neuron fires once and therefore a contribution of $(N-1)\epsilon$ to due the ensemble dynamics. Combining the two terms we get

$$L \leq 1 + (N-1)\epsilon + p(\tau - t_{ref}), \tag{B.7}$$

which we can transform into a condition for τ

$$\tau \geq \hat{\tau}_{min} = t_{ref} + \frac{L - 1 - (N-1)\epsilon}{p} = t_{ref} + \frac{(N-1)\epsilon(\eta - 1)}{p} \ . \tag{B.8}$$

Comparing this result with equation (2.5), we observe that $\hat{\tau}_{min} = \tau_{mf}$ and have thus found that the formulas (2.5) are a lower bound for the ISI τ. This bound of course can be improved for for $\eta < 1$, since there $\hat{\tau}_{min}$ is negative, although τ can never be smaller than t_{ref}. We use therefore the Heaviside step function and get

$$\tau_{min} = t_{ref} + \Theta\left(\frac{(N-1)\epsilon(\eta - 1)}{p}\right), \tag{B.9}$$

which is a lower bound for τ valid for all values of η.

B.3 Minimum mean ISI $\langle \tau \rangle_{min}$

To derive a lower bound for $\langle \tau \rangle$ we start with

$$
\begin{aligned}
\frac{N\delta}{\tau} &= g(\tau)\lfloor k_{min}(\tau) + 1 \rfloor \\
&\leq g(\tau)\left((N-1)(1-\eta) + \frac{p(\tau - 1 - t_{ref})\Theta(\tau - 1 - t_{ref})}{\epsilon} + 1\right), \tag{B.10}
\end{aligned}
$$

which can be obtained from (4.6), (4.7) and (A.3). We calculate the mean of the left and right hand side according to the probabilities $P(\tau)$, which denominate the probability of the system ending up in a system with ISI τ.

$$\sum_{i=1}^{\tau_{max}} \frac{N\delta}{i} P(i) \leq \sum_{i=1}^{\tau_{max}} g(i) \left((N-1)(1-\eta) + \frac{p(i-1-t_{ref})\Theta(i-1-t_{ref})}{\epsilon} + 1 \right) P(i) \, .$$

(B.11)

We set $1/\tau = f$ where f is the spiking-frequency, use $P(\tau) = P(f) = P(g(\tau))$, eliminate the terms of the summation which equal 0 and get

$$
\begin{aligned}
N\langle f\rangle\delta \;\; \leq \;\; & \langle g\rangle \left((N-1)(1-\eta) + 1 - \frac{(1+t_{ref})p}{\epsilon} \right) + \\
& + \frac{p}{\epsilon} \left(\sum_{i=1}^{1+t_{ref}} g(i)P(i) + \sum_{i=2+t_{ref}}^{\tau_{max}} g(i)iP(i) \right) .
\end{aligned}
$$

(B.12)

Using the following identity $\langle XY\rangle = \langle X\rangle\langle Y\rangle + \mathrm{Cov}(X,Y)$ for two random variables X and Y we achieve

$$
\begin{aligned}
N\langle f\rangle\delta \;\; \leq \;\; & \langle g\rangle \left((N-1)(1-\eta) + 1 - \frac{(1+t_{ref})p}{\epsilon} \right) + \\
& + \frac{p}{\epsilon} \left(\langle g\rangle\langle\tau\rangle + \mathrm{Cov}(g(\tau),\tau) - \sum_{i=2}^{1+t_{ref}} g(i)(i-1)P(i) \right) .
\end{aligned}
$$

(B.13)

From (B.10) it is easy to see that $\mathrm{Cov}(g(\tau),\tau) \leq 0$ since an increase of τ translates into a decrease of $g(\tau)$ and vice versa. Because of this fact and $g(\tau) \geq 0$ we can eliminate the two leftmost terms of inequality (B.13) by weakening the inequality.

$$N\langle f\rangle\delta \leq \langle g\rangle \left((N-1)(1-\eta) + 1 + \frac{p(\langle\tau\rangle - 1 - t_{ref})}{\epsilon} \right) .$$

(B.14)

The mean frequency $\langle f\rangle$ is equal to the inverse of the harmonic mean $h(\tau)$. Since for a set of positive numbers its harmonic mean is never greater than its arithmetic mean (Bullen, 2003) we have $\frac{1}{\langle\tau\rangle} \leq \frac{1}{h(\tau)} = \langle f\rangle$. Applying this on inequality (B.14) leads to

$$\frac{N\delta}{\langle\tau\rangle} \leq \langle g\rangle \left((N-1)(1-\eta) + 1 + \frac{p(\langle\tau\rangle - 1 - t_{ref})}{\epsilon} \right) .$$

(B.15)

We can transform this into a quadratic inequality of $\langle\tau\rangle$ since $\langle\tau\rangle > 0$. It has the only positive solution

$$
\begin{aligned}
\langle\tau\rangle \geq \langle\tau\rangle_{min} \;\; = \;\; & \frac{(N-1)\epsilon(\eta-1)-\epsilon}{2p} + \frac{1+t_{ref}}{2} + \\
& + \sqrt{\left(\frac{(N-1)\epsilon(\eta-1)-\epsilon}{2p} + \frac{1+t_{ref}}{2} \right)^2 + \frac{N\epsilon\delta}{p\langle g\rangle}} \, .
\end{aligned}
$$

(B.16)

We have found a lower bound for the mean value of our ISI distribution.

Appendix C   Thermodynamic limits of $\langle\tau\rangle_{min}$ and τ_{max}

In this appendix we will calculate the thermodynamic limit (i.e. the behavior for $N \to \infty$) of $\langle\tau\rangle$ for the different regions of η. We first calculate the thermodynamic limits

of the bounds $\langle \tau \rangle_{min}$ and τ_{max} of $\langle \tau \rangle$ calculated in appendix B and then situate the thermodynamic limit of $\langle \tau \rangle$ between the limits of the bounds.

We start with the limit for $\langle \tau \rangle_{min}$ using (B.16):

- $\eta > 1$

$$
\begin{aligned}
\lim_{N \to \infty} \frac{\langle \tau \rangle_{min}}{N} &= \lim_{N \to \infty} \frac{\epsilon(\eta-1)}{2p} - \frac{\epsilon(\eta-1)}{2pN} + \frac{1+t_{ref}}{2N} + \\
&\quad + \sqrt{\left(\frac{\epsilon(\eta-1)}{2p} - \frac{\epsilon(\eta-1)}{2pN} + \frac{1+t_{ref}}{2N} \right)^2 + \frac{\epsilon\delta}{p\langle g \rangle N}} \\
&= \frac{\epsilon(\eta-1)}{2p} + \left| \frac{\epsilon(\eta-1)}{2p} \right|,
\end{aligned}
\tag{C.1}
$$

which for $\eta > 1$ is

$$
\lim_{N \to \infty} \frac{\langle \tau \rangle_{min}}{N} = \frac{\epsilon(\eta-1)}{p} \ .
\tag{C.2}
$$

This coincides with the limit of τ_{mf}/N (See equation (2.5)).

- $\eta = 1$

Setting $\eta = 1$ in (B.16) leads to

$$
\lim_{N \to \infty} \frac{\langle \tau \rangle_{min}}{\sqrt{N}} = \lim_{N \to \infty} \frac{1+t_{ref}}{2\sqrt{N}} - \frac{\epsilon}{2p\sqrt{N}} + \sqrt{\frac{1}{4N}\left(1+t_{ref} - \frac{\epsilon}{p}\right)^2 + \frac{\epsilon\delta}{p\langle g \rangle}} = \sqrt{\frac{\epsilon\delta}{p\langle g \rangle}}.
\tag{C.3}
$$

- $\eta < 1$

Equation (C.1) for $\eta < 1$ leads to $\lim_{N\to\infty} \langle \tau \rangle_{min}/N = 0$, but we can improve this result. We transform (B.16) slightly and calculate

$$
\begin{aligned}
\lim_{N \to \infty} \langle \tau \rangle_{min} &= \lim_{N \to \infty} \frac{1+t_{ref}}{2} - \frac{(N-1)\epsilon(1-\eta)+\epsilon}{2p} + \\
&\quad + \sqrt{\left(\frac{(N-1)\epsilon(1-\eta)+\epsilon}{2p} - \frac{1+t_{ref}}{2} \right)^2 + \frac{N\epsilon\delta}{p\langle g \rangle}} \ .
\end{aligned}
$$

Applying $-a + b = \frac{-a^2+b^2}{a+b}$ we get

$$
\begin{aligned}
\lim_{N \to \infty} \langle \tau \rangle_{min} &= \lim_{N \to \infty} \frac{\frac{N\epsilon\delta}{p\langle g \rangle}}{\frac{(N-1)\epsilon(1-\eta)+\epsilon}{2p} - \frac{1+t_{ref}}{2} + \sqrt{\left(\frac{(N-1)\epsilon(1-\eta)+\epsilon}{2p} - \frac{1+t_{ref}}{2} \right)^2 + \frac{N\epsilon\delta}{p\langle g \rangle}}} \\
&= \delta \left(\frac{\langle g \rangle(1-\eta)}{2} + \left| \frac{\langle g \rangle(1-\eta)}{2} \right| \right)^{-1}
\end{aligned}
\tag{C.4}
$$

and have therefore for $\eta < 1$

$$
\lim_{N \to \infty} \langle \tau \rangle_{min} = \frac{\delta}{\langle g \rangle(1-\eta)} \ .
\tag{C.5}
$$

The limits for τ_{max} can be calculated analogously from equation (B.3). Combining the limits for both bounds with the result of equation (B.6) that the system has an ISI of δ for $\eta < 0.5$ we obtain

$$\lim_{N\to\infty} \langle\tau\rangle = \delta \qquad\qquad \text{if } \eta < 0.5 \;,$$

$$\frac{\delta}{\langle g\rangle(1-\eta)} \leq \lim_{N\to\infty} \langle\tau\rangle \leq \frac{\delta}{(1-\eta)} \qquad\qquad \text{if } 0.5 \leq \eta < 1 \;,$$

$$\sqrt{\frac{\epsilon\delta}{p\langle g\rangle}} \leq \lim_{N\to\infty} \frac{\langle\tau\rangle}{\sqrt{N}} \leq \sqrt{\frac{\epsilon\delta}{p}} \qquad\qquad \text{if } \eta = 1 \;,$$

$$\lim_{N\to\infty} \frac{\langle\tau\rangle}{N} = \frac{\epsilon(\eta-1)}{p} \qquad\qquad \text{if } \eta > 1 \;. \tag{C.6}$$

Acknowledgements

References

Abeles, M. (1991). *Corticonics: Neural circuits of the cerebral cortex*. Cambridge: Cambridge University Press.

Bienenstock, E. (1995). A model of neocortex. *Network-Computation In Neural Systems*, *6*, 179–224.

Bolle, D. & Blanco, J. B. (2004). Two-cycles in spin-systems: sequential versus synchronous updating in multi-state ising-type ferromagnets. *European Physical Journal B*, *42*, 397–406.

Brunel, N. & Hakim, V. (1999). Fast global oscillations in networks of integrate-and-fire neurons with low firing rates. *Neural Computation*, *11*, 1621–1671.

Brunel, N. & Hansel, D. (2006). How noise affects the synchronization properties of recurrent networks of inhibitory neurons. *Neural Computation*, *18*, 1066–1110.

Buck, J. (1988). Synchronous rhythmic flashing of fireflies .II. *Quarterly Review Of Biology*, *63*, 265–289.

Bullen, P. S. (2003). *Handbook of Means and Their Inequalities*. Dordrecht, The Netherlands: Kluwer.

Burkitt, A. N. (2006). A review of the integrate-and-fire neuron model: I. homogeneous synaptic input. *Biological Cybernetics*, *95(1)*, 1–19.

Burkitt, A. N. & Clark, G. M. (1999). Analysis of integrate-and-fire neurons: Synchronization of synaptic input and spike output. *Neural Computation*, *11(4)*, 871–901.

Campbell, S. R., Wang, D. L. L. & Jayaprakash, C. (1999). Synchrony and desynchrony in integrate-and-fire oscillators. *Neural Computation*, *11*, 1595–1619.

Chen, C. C. (1994). Threshold effects on synchronization of pulse-coupled oscillators. *Physical Review E*, *49*, 2668–2672.

Copeland, J. & Moiseff, A. (1995). The occurrence of synchrony in the north-american firefly photinus-carolinus (coleoptera, lampyridae). *Journal Of Insect Behavior*, *8*, 381–394.

Diesmann, M., Gewaltig, M. O. & Aertsen, A. (1999). Stable propagation of synchronous spiking in cortical neural networks. *Nature*, *402*, 529–533.

Durstewitz, D., Seamans, J. K. & Sejnowski, T. J. (2000). Neurocomputational models of working memory. *Nature Neuroscience Supplement*, *3*, 1184–1191.

Ernst, U., Pawelzik, K. & Geisel, T. (1998). Delay-induced multistable synchronization of biological oscillators. *Physical Review E*, *57*, 2150–2162.

Fontanari, J. F. & Köberle, R. (1988). Information-processing in synchronous neural networks. *Journal de Physique*, *49*, 13–23.

Fusi, S. & Mattia, M. (1999). Collective behavior of networks with linear (vlsi) integrate and fire neurons. *Neural Computation*, *11*, 633–652.

Gerstein, G. L. & Mandelbrot, B. (1964). Random walk models for the spike activity of a single neuron. *Biophys J*, *4*, 41–68.

Gerstner, W. (2000). Population dynamics of spiking neurons: Fast transients, asynchronous states, and locking. *Neural Computation*, *12*, 43–89.

Gómez, V., Kaltenbrunner, A. & López, V. (2006). Event modeling of message interchange in stochastic neural ensembles. In *IJCNN'06 Proceedings* (pp. 81–88). IEEE World Congress of Computational Intelligence, Vancouver, BC, Canada.

Herz, A. V. M. & Marcus, C. M. (1993). Distributed dynamics in neural networks. *Physical Review E*, *47*, 2155–2161.

Hong, Y. W. & Scaglione, A. (2005). A scalable synchronization protocol for large scale sensor networks and its applications. *IEEE Journal On Selected Areas In Communications*, *23*, 1085–1099.

Ikegaya, Y., Aaron, G., Cossart, R., Aronov, D., Lampl, I., Ferster, D. & Yuste, R. (2004). Synfire chains and cortical songs: Temporal modules of cortical activity. *Science*, *304*, 559–564.

Izhikevich, E. M. (2006). Polychronization: Computation with spikes. *Neural Computation*, *18*, 245–282.

Izhikevich, E. M., Gally, J. A. & Edelman, G. M. (2004). Spike-timing dynamics of neuronal groups. *Cerebral Cortex*, *14*, 933–944.

Kaneko, K. (1990). Clustering, coding, switching, hierarchical ordering, and control in a network of chaotic elements. *Physica D*, *41*, 137–172.

Kirk, V. & Stone, E. (1997). Effect of a refractory period on the entrainment of pulse-coupled integrate-and-fire oscillators. *Physics Letters A*, *232*, 70–76.

Kuramoto, Y. (1984). *Chemical oscillations, waves and turbulence.* Springer, Berlin.

Lindner, B. (2004). Interspike interval statistics of neurons driven by colored noise. *Physical Review E, 69*, 022901.

McMillen, D. & Kopell, N. (2003). Noise-stabilized long-distance synchronization in populations of model neurons. *Journal of Computational Neuroscience, 15*, 143–157.

Middleton, J. W., Chacron, M. J., Lindner, B. & Longtin, A. (2003). Firing statistics of a neuron model driven by long-range correlated noise. *Physical Review E, 68*, 021920.

Mirollo, R. E. & Strogatz, S. H. (1990). Synchronization of pulse-coupled biological oscillators. *SIAM Journal on Applied Mathematics, 50(6)*, 1645–1662.

Néda, Z., Ravasz, E., Brechet, Y., Vicsek, T. & Barabási, A. L. (2000). The sound of many hands clapping - tumultuous applause can transform itself into waves of synchronized clapping. *Nature, 403*, 849–850.

Östborn, P. (2002). Phase transition to frequency entrainment in a long chain of pulse-coupled oscillators. *Physical Review E, 66*, 016105.

Östborn, P., Åberg, S. & Ohlén, G. (2003). Phase transitions towards frequency entrainment in large oscillator lattices. *Physical Review E, 68*, 015004.

Peskin, C. (1975). *Mathematical aspects of heart physiology.* New York: Courant Institute of Mathematical Sciences, New York University.

Rhouma, M. B. H. & Frigui, H. (2001). Self-organization of pulse-coupled oscillators with application to clustering. *IEEE Transactions On Pattern Analysis And Machine Intelligence, 23*, 180–195.

Rodríguez, F., Suárez, A. & López, V. (2001). Period focusing induced by network feedback in populations of noisy integrate-and-fire neurons. *Neural Computation, 13*, 2495–2516.

Rodríguez, F., Suárez, A. & López, V. (2002). A discrete model of neural ensembles. *Philosophical Transactions of The Royal Society: Mathematical, Physical and Engineering Sciences, 360*, 559–573.

Salinas, E. & Sejnowski, T. J. (2002). Integrate-and-fire neurons driven by correlated stochastic input. *Neural Computation, 14*, 2111–2155.

Senn, W. & Urbanczik, R. (2000). Similar nonleaky integrate-and-fire neurons with instantaneous couplings always synchronize. *SIAM Journal On Applied Mathematics, 61*, 1143–1155.

Stein, R. B. (1967). Some models of neuronal variability. *Biophysical Journal, 7*, 37–68.

Timme, M., Wolf, F. & Geisel, T. (2002). Prevalence of unstable attractors in networks of pulse-coupled oscillators. *Physical Review Letters, 89(15)*, 154105.

Tuckwell, H. C., Cannings (editor), C., Hoppensteadt(editor), F. & Segel (editor), L. A. (1988). *Introduction to Theoretical Neurobiology: Volume 2, Nonlinear and stochastic theories.* Cambridge University Press, Cambridge.

van Vreeswijk, C. (1996). Partial synchronization in populations of pulse-coupled oscillators. *Physical Review E, 54*, 5522–5537.

van Vreeswijk, C. & Abbott, L. F. (1993). Self-sustained firing in populations of integrate-and-fire neurons. *SIAM Journal On Applied Mathematics, 53*, 253–264.

Wang, X. J. (2001). Synaptic reverberation underlying mnemonic persistent activity. *Trends In Neurosciences, 24*, 455–463.

Winfree, A. (1967). Biological rhythms and the behavior of populations of coupled oscillators. *J. Theoret. Biol., 16*, 15–42.